THE JOURNAL OF PHYSICAL CHEMISTRY A
A JOURNAL OF THE AMERICAN CHEMICAL SOCIETY

pubs.acs.org/JPCA

Feature Article

The Local Vibrational Mode Theory and Its Place in the Vibrational Spectroscopy Arena

Elfi Kraka,* Mateus Quintano, Hunter W. La Force,‡ Juliana J. Antonio,‡ and Marek Freindorf

Cite This: *J. Phys. Chem. A* 2022, 126, 8781−8798

Read Online

ACCESS | Metrics & More | Article Recommendations | Supporting Information

ABSTRACT: This Feature Article starts highlighting some recent experimental and theoretical advances in the field of IR and Raman spectroscopy, giving a taste of the breadth and dynamics of this striving field. The local mode theory is then reviewed, showing how local vibrational modes are derived from fundamental normal modes. New features are introduced that add to current theoretical efforts: (i) a unique measure of bond strength based on local mode force constants ranging from bonding in single molecules in different environments to bonding in periodic systems and crystals and (ii) a new way to interpret vibrational spectra by pinpointing and probing interactions between particular bond stretching contributions to the normal modes. All of this represents a means to work around the very nature of normal modes, namely that the vibrational motions in polyatomic molecules are delocalized. Three current focus points of the local mode analysis are reported, demonstrating how the local mode analysis extracts important information hidden in vibrational spectroscopy data supporting current experiments: (i) metal−ligand bonding in heme proteins, such as myoglobin and neuroglobin; (ii) disentanglement of DNA normal modes; and (iii) hydrogen bonding in water clusters and ice. Finally, the use of the local mode analysis by other research groups is summarized. Our vision is that in the future local mode analysis will be routinely applied by the community and that this Feature Article serves as an incubator for future collaborations between experiment and theory.

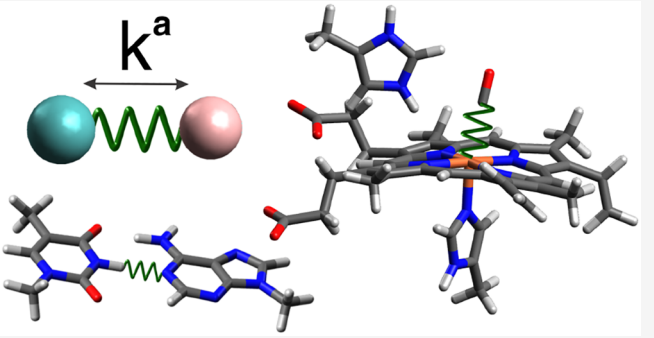

INTRODUCTION

Over the past two decades, vibrational spectroscopy has developed into an important tool with ample applications in chemistry and beyond.[1−8] The number of available high precision measured and calculated vibrational spectra is constantly increasing thanks to rapidly advancing technologies and computational methods. To demonstrate this, in the following, some recent experimental and theoretical advances will be highlighted rather than giving a complete overview of this dynamic and complex field in all its breadth, which would be far beyond the scope of a feature article.

Recent Experimental Advances. *Infrared (IR) Spectroscopy.* The reach of infrared (IR) spectroscopy has extended across gas and condensed phases via measurements in near- (ca. 4000−14000 cm^{-1}), mid- (ca. 400−4000 cm^{-1}), and far- (ca. 10−400 cm^{-1}) infrared regions of the electromagnetic spectrum.[9−12] Considerable progress has been made toward experimental techniques,[12,13] in synergy with new theoretical/computational methods supporting the interpretation of spectral features with increasing degree of complexity.[9,11,14−16] One application toward modeling protein IR spectra comes in the form of the python package AIM,[17] created for the visualization of protein amide-I band, which provides information on a protein's secondary structure. Recently, researchers have been able to investigate proteins with conformational heterogeneity with the use of Markov state models and calculated IR spectra.[18] Fourier Transform IR (FTIR) is a practical tool to observe structural changes in small cells and other biochemical parameters in tissue samples.[19−21] Vibrational sum-frequency generation (SFG) spectroscopy has demonstrated a unique capability to probe previously hidden protein conformational dynamics at solid/liquid interfaces, as well as amide-I spectra with a frequency equivalent to a concurrent IR and visible signal.[22−25] Chiral SFG also has implications in distinguishing secondary structures of biomolecules and can solve biological problems related with chiral selectivity of biomolecular interactions at the molecular level.[26−28]

Raman Spectroscopy. For IR inactive compounds the inelastic scattering of light (Raman scattering) provides a powerful alternative. Of late, the experimental applications of probing vibrational modes with Raman spectroscopy has been expanded from food,[13] condensed phases,[11] textile,[29,30]

Received: August 19, 2022
Revised: October 20, 2022
Published: November 8, 2022

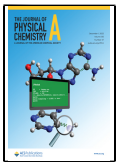

https://doi.org/10.1021/acs.jpca.2c05962
J. Phys. Chem. A 2022, 126, 8781−8798

catalysts,[6] and biomedical purposes.[31,32] Some advances that go beyond standard Raman methods include the surface-enhanced Raman spectroscopy (SERS), photoinduced enhanced Raman spectroscopy (known as PIERS), low-frequency Raman spectroscopy (LFR) and tip-enhanced Raman spectroscopy (TERS). This list is not meant to be exhaustive, but cover a basic overview of techniques that have been generally more favored in the scientific community. SERS has very recently gained increasing interest for its ability to rapidly probe target molecules noninvasively with high-selectivity and ultrahigh sensitivity.[33] This is due to both chemical contributions and electromagnetic enhancement contributions. The interaction between the plasmonic nanostructure surface and the molecule(s) absorbed on it can lead to an average enhancement range from 10^4−10^6 orders of magnitude.[34] TERS, on the other-hand, has a near-field approach, and based on the metal tip of TERS, the spatial resolution can be significantly improved and reach a resolution of about 10 nm.[35] Recently, experimentalists have used both SERS/TERS to uncover the landscape of protein post-translational modification,[36] altercations of red blood cells and organs at the molecular level[37−39] and the identification of the "S" and "N" proteins in SARS-CoV-2.[40] Also, the irradiation of light on a substance without any other manipulation can lead to an enhancement of several to a dozen times over SERS.[41] Despite having some overlap of the spectral threshold with regards to LFR, narrow wavelength band filters have been suggested to enhance the applicability, albeit allowing only for basic characterization.[42] Most of these enhanced instrumentations have been able to describe vibrational motions (with normal modes), and some have even been used to characterize structural configurations, such as enantiomers.[43] Understanding and modeling protein conformational dynamics is a critical area of interest for both clinical and computational sectors,[31,44] where both Raman and IR spectroscopy have been used to elicit the dynamic behaviors of proteins.[25,36,45]

Periodic/Condensed Phase Systems. For periodic and condensed phase systems, vibrational spectroscopy can lead to a plethora of valuable information regarding long-range interactions[46] and collective dynamics[47] (such as hydration and kinetics). Terahertz (THz) spectroscopy has a range of about 0.1−10 THz (3−300 cm^{-1}) and has become a popular choice for the investigation of condensed phase systems. The caveat of using these techniques is the lack of specific functional-group transition,[46] which generally means the use of these experimental techniques needs to be paired with advanced computational methods.[11,48] The problem that arises with condensed systems is the ability to provide vibrational modes that have accurate vibrational assignments without mixed mode coupling,[49] even with utilizing powerful periodic density functional theory methods. This also can apply for electrochemical materials, especially since the closed configurations do not involve gaseous species in the redox reaction of sealed cell batteries.[4] For crystals, a recent publication with the use of Raman scattering techniques displays the inconsistency of using even second-order vibrational modes to describe structural characteristics, since there are overlaps that complicate structural assignment.[50]

Theoretical Advances. Computational vibrational spectroscopy has emerged as an independent, highly specialized quantum chemistry subfield, complementing experimental efforts with a rich variety of information regarding spectroscopic properties and features, as well as predicting spectroscopic data about compounds not being amenable to experiment (i.e., unstable and/or toxic compounds, or compounds suggested to exist in space). The calculation of vibrational frequencies requires the second energy derivative matrix (Hessian) evaluated at a local or global energy minimum (i.e., stationary point) on the potential energy surface (PES), which serves as input for the so-called *normal-mode analysis* (NMA), providing normal-mode frequencies and corresponding normal modes.[51] A more detailed discussion is given in the methodology section. Standard methods generally work within the harmonic approximation of the PES leading to harmonic vibrational frequencies.[52] Algorithms for NMA and harmonic frequency calculations have been integrated in many commercial/non-commercial electronic structure software packages such as QCHEM, GAMESS, GAUSSIAN, MOLPRO, HyperChem, etc., and as such, are routinely used by the community. On the lower-accuracy end, frequency calculations are typically performed with classical molecular mechanics (MM) methods being based on force field parameters either fitted by experimental data or from *ab initio* calculations,[53] on the higher-end of the spectrum, quantum chemical (QM) methods are applied ranging from Hartree−Fock (HF),[54] density functional theory (DFT) approaches,[55,56] to expensive post-HF wave function methods.[9,14] DFT methods are a popular choice because they are easy to use, providing analytical second energy derivatives, and depending on the level of functional used, are computationally accessible even for larger systems. On the other hand, the choice of functional can strongly influence the accuracy of the calculated vibrational data.[57] Therefore, one has to be mindful to select the appropriate functional for the system under consideration, especially when calculating vibrational properties for systems with noncovalent interactions.[58] Hybrid QM/MM methods that combine quantum mechanical descriptions with classical models have become a popular compromise for large systems.[59] First-principles molecular dynamics (FPMD) simulations have emerged as an attractive method for the simulation of vibrational spectra. They explicitly treat the vibrational motion present in a compound and have proven to provide a realistic description of large and condensed systems subject to complex intramolecular and intermolecular interactions.[7,60−63] Statistical thermodynamics (in its quantum-mechanical form) can be used for accurately predicting vibrational thermodynamic properties by means of vibrational frequencies.[64]

Beyond the Harmonic Approximation. Although the harmonic approximation is undeniably useful both quantitatively and qualitatively and scaling procedures may help to get closer to the experimental picture,[65] there are scenarios when the accuracy needs to extend beyond the harmonic approximation. The use of anharmonic corrections to the PES has been shown to create complications with the solution of the Schrödinger equation. One way around this is to use vibrational perturbation theory to the second order (VPT2), since the vibrational states can be computed with respect to normal modes.[14] Utilizing VPT2, Morgan et al.[66] was able to accurately provide fundamental modes using a small PES grid of a prototypical tetra-atomic system. Interestingly, a derivation of fourth-order vibrational perturbation (VPT4) was based on the Watson Hamiltonian in dimensionless rectilinear normal coordinates and applications for this include semiclassical transition state theory.[67] Vibrational configuration interaction (VCI) in combination with vibrational self-consistent field methods (VCI-VSCF)[14] or ab initio molecular dynamics (AIMD)[68] are frequently used alternatives. Newer coarse-

https://doi.org/10.1021/acs.jpca.2c05962
J. Phys. Chem. A 2022, 126, 8781−8798

grained methods, such as "rectangular collocation', have been shown to produce frequencies within 1 cm^{-1} of experiment without the need for a defined PES, largely decreasing the computational bottleneck for complex systems often found when observing molecule−surface interactions.[69] On a separate note, Fortenberry and Lee[70] have described quartic force fields (QFFs) as defining the potential portion of the internuclear Hamiltonian. This QFFs methodology was used to represent rotational constants that are chemically computed with a condition that the molecules of interest have two or more heavy atoms.[71] With this, they benchmarked predicted fundamental vibrational frequencies within 5.7 cm^{-1} from the experiment.

Machine-Learning-Based Methods. Machine learning (ML) methods have classified a new frontier of computational chemistry, bridging the gaps formed by vibrational analysis and structural analysis, with the potential for predicting spectral motifs and generating vibrational maps[17,72,73] for a series of compounds at a time. There are several strategies with varying degrees of utility when it comes to simulating chemical environments and vibrational spectra in ML, such as artificial neural networks (ANN),[74,75] autoencoders (AE),[76] Gaussian process regression (GPR) models,[73] and several others.[33] These models not only have been used to isolate spectral signals and eliminate congestion in complex spectra,[77] but they have also been used to expand the computational limit of simulating macro-scale dynamics at the quantum level.[78] Generally, machine learning algorithms involve a step to learn intrinsic behaviors and patterns of the system known as "training", a validation step to assess the success of the training and tune the hyperparameters, and a testing step where new information is fed to the model and the generative aspect of these models become apparent.[79] Factors that diminish the current successes of these models include poor model generalizability and an intrinsic reliance on the training set or level of theory that was used to generate the model.[80] On the other hand, these models have seen a wide array of uses in the field of computational chemistry, including force fields,[78] excited state dynamics,[81] and simulating solvent effects in IR spectra.[82] ML methods have recently gained attention for their use in constructing vibrational spectra from MD/AIMD trajectories,[83−85] and this direction shows promise for elucidating the spectral connection for complex chemical systems.

Overall, there have been considerable advances in the field of vibrational spectroscopy, both concerning experiment and theory. However, what has been missing is a quantitative measure of bond strength based on vibrational spectroscopy data and a way to unravel the rich information contained in an IR/Raman spectrum. This is what the local vibrational mode theory adds to the toolbox.

LOCAL VIBRATIONAL MODE THEORY

In the following, the essence of our local vibrational mode theory and its place in the field of theoretical vibrational spectroscopy[8,86−88] is summarized; a comprehensive review is given in ref 89 based on the original work of Konkoli-Cremer.[90−94]

Normal Mode Analysis and Wilson GF Formalism. Starting from the force constant matrix $\mathbf{F}$, information about the N_{vib} ($N_{vib} = 3N - N_{tr}$, and $N_{tr} = 5$ or 6 for linear and nonlinear molecules with N atoms) vibrational frequencies and how the atoms move under a certain vibration can be retrieved from solving the vibrational secular equation.[86−88] Expressed in Cartesian coordinates this equation takes the form

$$\mathbf{F}^x\tilde{\mathbf{L}} = \mathbf{M}\tilde{\mathbf{L}}\mathbf{\Lambda} \tag{1}$$

where matrix $\tilde{\mathbf{L}}$ collects the N_{vib} vibrational eigenvectors $\tilde{\mathbf{l}}_\mu$ in its columns. $\mathbf{\Lambda}$ is a diagonal matrix with the eigenvalues λ_μ, connected to the harmonic vibrational frequencies ω_μ according to $\lambda_\mu = 4\pi^2c^2{\omega_\mu}^2$, and c is the speed of light. $\mathbf{M}$ is the diagonal mass matrix of the molecule in question which contains each atomic mass three times to account for the motion in the x, y, and z direction, respectively, i.e., $M_{i,i} = \{m_1, m_1, m_1, m_2, m_2, m_2, ...\}$. The tilde above a vector or matrix symbol indicates mass-weighting. Matrix $\tilde{\mathbf{L}}$ has the following properties

$$\tilde{\mathbf{L}}^\dagger\mathbf{M}\tilde{\mathbf{L}} = \mathbf{I} \tag{2}$$

$$\tilde{\mathbf{L}}^\dagger\mathbf{F}^x\tilde{\mathbf{L}} = \mathbf{\Lambda} \tag{3}$$

i.e., matrix $\tilde{\mathbf{L}}$ and eigenvalue matrix $\mathbf{\Lambda}$ are obtained by diagonalization of the force constant matrix. Usually, the normal mode vectors $\tilde{\mathbf{l}}_\mu$ are renormalized according to

$$\mathbf{l}_\mu = \frac{1}{\sqrt{\tilde{\mathbf{l}}_\mu^\dagger\tilde{\mathbf{l}}_\mu}}\tilde{\mathbf{l}}_\mu = \sqrt{m_\mu^R}\,\tilde{\mathbf{l}}_\mu \tag{4}$$

where $m_\mu^R = (\tilde{\mathbf{l}}_\mu^\dagger\tilde{\mathbf{l}}_\mu)^{-1}$ is the reduced mass of mode μ. Eq 4 expressed in matrix form leads to $\mathbf{L} = \tilde{\mathbf{L}}(\mathbf{M}^R)^{1/2}$.

Matrix $\mathbf{L}$ also satisfies eq 1, which leads to

$$\mathbf{L}^\dagger\mathbf{F}^x\mathbf{L} = \mathbf{K} \tag{5}$$

$$\mathbf{L}^\dagger\mathbf{M}\mathbf{L} = \mathbf{M}^R \tag{6}$$

Eqs 5 and 6 define the diagonal normal force constant matrix $\mathbf{K}$ and the reduced mass matrix $\mathbf{M}^R$ (with elements m_μ^R), respectively. Eq 5 leads to the transformation of the Cartesian coordinates to normal coordinates $\mathbf{Q}$, which together with the normal modes and the force constant matrix $\mathbf{K}$ forms the basis for the normal-mode analysis; an integral part of all modern quantum chemistry packages calculating vibrational frequencies.[95] The vibrational secular equation expressed in internal coordinates q_n is given by[86]

$$\mathbf{F}^q\tilde{\mathbf{D}} = \mathbf{G}^{-1}\tilde{\mathbf{D}}\mathbf{\Lambda} \tag{7}$$

$\tilde{\mathbf{D}}$ contains the normal mode vectors $\tilde{\mathbf{d}}_\mu$ ($\mu = 1, ..., N_{vib}$). The real symmetric matrix $\mathbf{G}$ is the Wilson $\mathbf{G}$ matrix,[86] also called the *inverse kinetic energy* matrix, with off-diagonal elements of the form $G_{ij} = G_{ji}$ describing the kinetic coupling between modes i and j.[86] Renormalization of $\tilde{\mathbf{D}}$ according to $\mathbf{D} = \tilde{\mathbf{D}}(\mathbf{M}^R)^{1/2}$ leads to

$$\mathbf{F}^q\mathbf{D} = \mathbf{G}^{-1}\mathbf{D}\mathbf{\Lambda} \tag{8}$$

$$\mathbf{D}^\dagger\mathbf{F}^q\mathbf{D} = \mathbf{K} \tag{9}$$

$$\mathbf{D}^\dagger\mathbf{G}^{-1}\mathbf{D} = \mathbf{M}^R \tag{10}$$

Cartesian and internal coordinate systems are connected by the following equations:

$$\mathbf{F}^\mathbf{q} = \mathbf{C}^\dagger\mathbf{F}^x\mathbf{C} \tag{11}$$

$$\mathbf{G} = \mathbf{B}\mathbf{M}^{-1}\mathbf{B}^\dagger \tag{12}$$

$$\mathbf{D} = \mathbf{B}\mathbf{L} \tag{13}$$

The rectangular Wilson $\mathbf{B}$ matrix provides the relationship between internal and Cartesian coordinates via the first

https://doi.org/10.1021/acs.jpca.2c05962
J. Phys. Chem. A 2022, 126, 8781−8798

derivatives of the internal coordinates q_n ($n = 1, 2, 3,..., N_{vib}$) with regard to the Cartesian coordinates x_i ($i = 1, 2, 3, ..., 3N$)

$$\mathbf{B}_n = \frac{\delta q_n(\mathbf{x})}{\delta x_i} \tag{14}$$

Important to note is that this can be extended to other coordinates, such as curvilinear coordinates describing ring inversion and bond pseudorotation in Jahn−Teller systems[96−98] and Cremer−Pople ring puckering coordinates,[99] or internal valence coordinates,[100] etc., as long as the $\mathbf{B}_n$ vector can be derived according to eq 14 for the coordinate n under consideration. The $\mathbf{B}$ matrix also provides the link between the $\mathbf{G}$ matrix and the diagonal mass matrix $\mathbf{M}$ matrix[86]

$$\mathbf{G} = \mathbf{B}\mathbf{M}^{-1}\mathbf{B}^{\dagger} \tag{15}$$

Matrix $\mathbf{C}$ is the general-inverse of the $\mathbf{B}$ matrix[86] defined by

$$\mathbf{C} = \mathbf{M}^{-1}\mathbf{B}^{\dagger}\mathbf{G}^{-1} \tag{16}$$

$$\mathbf{B}\mathbf{C} = \mathbf{I}_{N_{vib}} \tag{17}$$

It has to be noted that $\mathbf{C}\mathbf{B} \neq \mathbf{I}_{3N}$ since $\mathbf{B}$ is spanned in the N_{vib}-dimensional vibrational space only.

It is important to stress that normal coordinates $\mathbf{Q}$ are generally a linear combination of Cartesian or internal coordinates as shown by Wilson[101] providing the important link between normal and internal coordinates

$$\mathbf{q} = \mathbf{B}\mathbf{x} \text{ and } \mathbf{q} = \tilde{\mathbf{D}}\mathbf{Q} \tag{18}$$

Left multiplication of both sides of eq 18 by $\tilde{\mathbf{D}}^{\dagger}\mathbf{G}^{-1}$ leads to,

$$\mathbf{Q} = \tilde{\mathbf{D}}^{\dagger}\mathbf{G}^{-1}\mathbf{q} \tag{19}$$

with $\tilde{\mathbf{D}}^{\dagger}\mathbf{G}^{-1}\tilde{\mathbf{D}} = \mathbf{I}$.[101] A closer look at each entry (i.e., normal coordinate) Q_n of the amplitude vector in normal coordinates $\mathbf{Q}$ in eq 19 reveals

$$Q_n = \sum_{j}^{N_{vib}} (\tilde{D}^{\dagger}G^{-1})_{nj} q_j \tag{20}$$

Eq 20 provides the important mathematical proof that normal coordinates are linear combinations of internal coordinates obtained by the linear transformation of space represented by eq 19. Inserting $\mathbf{q} = \mathbf{B}\mathbf{x}$ into eq 19 provides the proof of Barone's, Puzzarini's, and co-workers' recent suggestion that normal coordinates can be expressed as linear combinations of Cartesian coordinates as well[14]

$$\mathbf{Q} = \tilde{\mathbf{D}}^{\dagger}\mathbf{G}^{-1}\mathbf{B}\mathbf{x} \tag{21}$$

Mass-Decoupled Euler−Lagrange Equations. Normal vibrational modes embed complex and rich information on the electronic structure of a molecule and its chemical bonds, ready to be decoded. However, as shown in eqs 19−21, they are generally delocalized in the case of polyatomic molecules as given by the nature of the normal coordinates. This can easily be visualized in a normal mode animation showing the normal mode as a collective motion of internal coordinates. To obtain information about a specific molecular fragment, in particular to derive a bond strength measure based on vibrational spectroscopy data, the normal vibrational modes have to be transformed into local vibrational modes describing a specific molecular fragment of interest. For this purpose, Konkoli and Cremer went back to the original theory of a vibrating molecule and derived in their seminal work[90−94] Euler−Lagrange equations for a molecular fragment ϕ_n being described by an internal parameter q_n while being independent of all the other internal coordinates q_m ($m \neq n$). They considered this fragment motion as a motion being obtained after relaxing all parts of the vibrating molecule but the fragment under consideration. Because of this property, they originally coined these modes *adiabatic internal coordinate modes*.[90,91] However, over the years for reasons of simplicity, the term *local modes* was adapted.[89]

In their ansatz, q_n is frozen at its equilibrium value $q_n^{\star}$ while the other coordinates q_m ($m \neq n$) can relax. At the minimum of the potential $V(\mathbf{q})$, then the following holds:

$$V(\mathbf{q}) = \min \tag{22}$$

$$q_n = q_n^{\star} \tag{23}$$

Eqs 22 and 23 can be solved using the method of Lagrange multipliers

$$\frac{\partial}{\partial q_m}[V(\mathbf{q}) - \lambda_n(q_n - q_n^{\star})] = 0 \quad m = 1, ..., N_{vib} \tag{24}$$

leading to N_{vib} Lagrange multipliers λ_n

$$\frac{\partial V(\mathbf{q})}{\partial q_m} = \lambda_n \delta_{mn} \quad m, n = 1, ..., N_{vib} \tag{25}$$

Eq 25 defines a one-dimensional subspace in the full vibrational space for each internal coordinate q_n. In this way, one obtains an internal, i.e., local vibrational mode associated with fragment ϕ_n.

It is important to note that the Euler−Lagrange equations are generally defined for any potential V, however the local vibrational mode theory is based on the harmonic approximation of the potential. After the solution of the vibrational problem in the harmonic approximation, the potential energy and each internal coordinate q_n can be expressed as functions of the N_{vib} normal coordinates Q_μ leading to the determination of the n Lagrange multipliers λ_n.

$$V(\mathbf{Q}) = \frac{1}{2}\sum_{\mu=1}^{N_{vib}} Q_\mu^{\dagger} k_\mu Q_\mu \tag{26}$$

$$q_n(\mathbf{Q}) = \sum_{\mu=1}^{N_{vib}} D_{n\mu} Q_\mu \tag{27}$$

$D_{n,\mu}$ is an element of the normal mode matrix $\mathbf{D}$ in the internal coordinate space and k_μ is the corresponding normal mode force constant. Eq 26 can be solved under the constraint $q_n = q_n^{\star}$, i.e., eq 23

$$\frac{\partial}{\partial Q_\mu}[V(\mathbf{Q}) - \lambda_n(q_n(\mathbf{Q}) - q_n^{\star})] = 0 \quad \mu = 1, ..., N_{vib} \tag{28}$$

leading to eqs 29 and 30

$$\frac{\partial V(\mathbf{Q})}{\partial Q_\mu} - \frac{\partial \lambda_n}{\partial Q_\mu}(q_n(\mathbf{Q}) - q_n^{\star}) - \lambda_n \frac{\partial (q_n(\mathbf{Q}) - q_n^{\star})}{\partial Q_\mu} = 0 \tag{29}$$

$$\frac{\partial V(\mathbf{Q})}{\partial Q_\mu} = \lambda_n \frac{\partial q_n(\mathbf{Q})}{\partial Q_\mu} \tag{30}$$

https://doi.org/10.1021/acs.jpca.2c05962
J. Phys. Chem. A 2022, 126, 8781−8798

considering that in eq 29 $q_n(\mathbf{Q}) = q_n^{\star}$ at an equilibrium, i.e., $(q_n(\mathbf{Q}) - q_n^{\star}) = 0$ and that $q_n^{\star}$ is a constant, i.e., $\frac{\partial q_n^{\star}}{\partial Q_\mu} = 0$. Insertion of eq 26 for $V(\mathbf{Q})$ and eq 27 for $q_n(\mathbf{Q})$ into eq 30 leads to

$$\frac{\partial}{\partial Q_\mu}\frac{1}{2}\sum_{\nu=1}^{N_{vib}} k_\nu Q_\nu^2 = \lambda_n \frac{\partial}{\partial Q_\mu}\sum_{\rho=1}^{N_{vib}} D_{n\rho} Q_\rho \tag{31}$$

and

$$k_\mu Q_\mu = \lambda_n D_{n\mu} \tag{32}$$

and for the μth normal coordinate

$$Q_\mu^{(n)} = \frac{D_{n\mu} k_\mu}{\lambda_n} \tag{33}$$

where the superscript (n) of $Q^{(n)}$ denotes a solution obtained under the constraint for $q_n = q_n^{\star}$. This leads to an expression for the Lagrange multipliers λ_n in terms of $q_n^{\star}$

$$q_n^{\star} = \sum_{\mu=1}^{N_{vib}} D_{n\mu} Q_\mu^{(n)} = \sum_{\mu=1}^{N_{vib}} \frac{D_{n\mu}^2}{k_\mu}\lambda_n \tag{34}$$

$$\lambda_n = \frac{1}{\sum_{\mu=1}^{N_{vib}} \frac{D_{n\mu}^2}{k_\mu}} q_n^{\star} \tag{35}$$

Inserting eq 35 into eq 33, one obtains the normal coordinate $Q_\mu^{(n)}$ as a function of $q_n^{\star}$

$$Q_\mu^{(n)} = \frac{\frac{D_{n\mu}}{k_\mu}}{\sum_{\nu=1}^{N_{vib}} \frac{D_{n\nu}^2}{k_\nu}} q_n^{\star} = Q_{\mu,n}^0 q_n^{\star} \tag{36}$$

with the constant $Q_{\mu,n}^0$ defining the μ-th component of the adiabatic vector in the normal coordinates

$$\mathbf{a}_n = (Q_{1,n}^0, Q_{1,n}^0, ..., Q_{\mu,n}^0, ...)^{\dagger} = \frac{\mathbf{K}^{-1}\mathbf{d}_n^{\dagger}}{\mathbf{d}_n\mathbf{K}^{-1}\mathbf{d}_n^{\dagger}} \tag{37}$$

Eq 37, which completely specifies the form of the adiabatic mode, implies the important result that all what is needed for the local mode analysis are the normal mode force constant matrix $\mathbf{K}$ and the normal mode vectors $\mathbf{d}_n$ in internal coordinates, i.e., the LMA analysis can be routinely performed after a standard vibrational frequency calculation via the Wilson GF formalism. The local mode vector $\mathbf{a}_n$ can be easily transformed into Cartesian coordinate space

$$\mathbf{a}_n^x = \mathbf{L}\mathbf{a}_n \tag{38}$$

where $\mathbf{L}$ is the normal mode matrix in Cartesian coordinates.[90−94]

Properties of Local Modes. Once the local mode vector $\mathbf{a}_n$, which determines the movement of the molecule under the influence of parameter is known, one can define molecular properties corresponding to this motion, such as local mode force constant, local mass and local frequency.[90−94]

The corresponding local force constant k_n^a of local mode n (superscript a denotes an adiabatically relaxed, i.e., local mode)[102] can be expressed as

$$k_n^a = \mathbf{a}_n^{\dagger}\mathbf{K}\mathbf{a}_n = \frac{1}{\mathbf{d}_n\mathbf{K}^{-1}\mathbf{d}_n^{\dagger}} \tag{39}$$

It has to be noted that the units of $\mathbf{B}$-matrix elements for bond lengths and bond angles are different, and as such the unit of bond length force constant k^a(AB) is mDyn/Å and the unit of a bond angle force constant k^a(ABC) is mDyn·Å/rad^2. The same is also true for other dihedral or curvilinear phase angles.[96] The associated local mass is defined as

$$m_n^a = \frac{1}{\mathbf{B}_n\mathbf{M}^{-1}\mathbf{B}_n^{\dagger}} = \frac{1}{G_{nn}} \tag{40}$$

where G_{nn} is a diagonal element of Wilson's $\mathbf{G}$ matrix.[86]

From the local mode force constant k_n^a and local mode mass m_n^a the local mode frequency can be calculated

$$(\omega_n^a)^2 = 1/(4\pi^2c^2)\frac{k_n^a}{m_n^a} = 1/(4\pi^2c^2)G_{nn}\mathbf{a}_n^{\dagger}\mathbf{K}\mathbf{a}_n \tag{41}$$

In addition, the local mode infrared intensity has been defined which can be related to bond dipole moments.[95]

Zou and Cremer[103] provided the important proof that the local stretching force constant k_n^a(AB) reflects the intrinsic strength of the bond/interaction between two atoms A and B being described by an internal coordinate q_n qualifying k_n^a(AB) as perfectly suited bond strength descriptor. It is convenient to base the comparison of the bond strength for larger sets of molecules on a chemically more prevalent relative bond strength (BSO n) rather than on a comparison of local force constant values. Both are connected via a power relationship of the form BSO $n = A(k_n^a)^B$ according to the generalized Badger rule derived by Cremer, Kraka and co-workers.[104,105] The constants A and B are calculated from k_n^a values of two reference compounds with known BSO n values and the requirement that for a force constant value of zero the corresponding BSO n value is zero. For example, for CC bonds suitable references are ethane and ethylene with BSO $n = 1$ and 2, respectively.[106] In the case of more complex bonding situations such as metal−ligand bonding, guidance by Mayer bond orders[107−109] can be utilized, as discussed below. Important to note is that reference molecules and target molecules should be described with the same model chemistry (i.e., method/basis set) to guarantee that the BSO n values compare well.

It is important to note that local vibrational frequencies and corresponding force constants can also be derived from measured fundamental normal-mode frequencies, which do not depend on any model chemistry used for the calculation, and even more importantly, which include anharmonicity effects not being captured by calculated harmonic frequencies.[110−112] The underlying assumption is that calculated normal mode vectors $\mathbf{d}_\mu$ are a reasonable approximation to the true normal mode vectors $\mathbf{d}'_\mu$. This assumption forms the basis for all frequency scaling procedures,[113−116] and therefore is well-founded. With $\mathbf{D}' \approx \mathbf{D}$ the true force constant matrix $\mathbf{F}^{q'}$ can be expressed via a perturbation added to the calculated $\mathbf{F}^q$ matrix, i.e., $\mathbf{F}^{q'} = \mathbf{F}^q + \Delta\mathbf{F}^q$, as shown by Konkoli and Cremer,[110,111]

$$(\mathbf{F}^q + \Delta\mathbf{F}^q)\mathbf{D} = \mathbf{G}^{-1}\mathbf{D}(\mathbf{\Lambda} + \Delta\mathbf{\Lambda}) \tag{42}$$

The perturbation matrix $\Delta\mathbf{F}^q$ can be obtained from

$$\Delta\mathbf{F}^q\mathbf{D} = \mathbf{G}^{-1}\Delta\mathbf{\Lambda} \tag{43}$$

https://doi.org/10.1021/acs.jpca.2c05962
J. Phys. Chem. A 2022, 126, 8781−8798

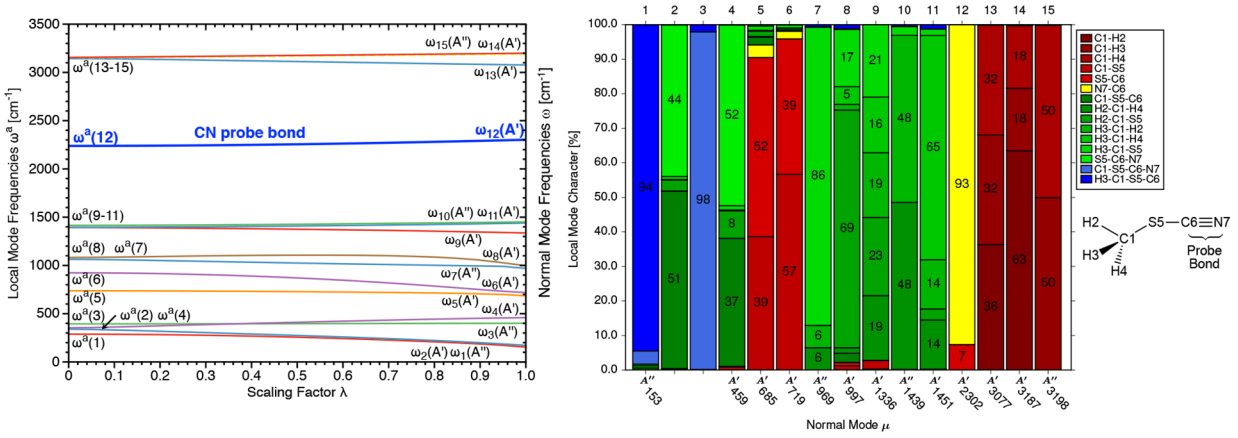

(a) (b)

Figure 1. (a) Adiabatic connection scheme and (b) decomposition of normal modes into local mode contributions for CH_3SCN: ωB97X-D/aug-cc-pVDZ level of theory.[122−124] Reprinted with permission from ref 89. Copyright 2020 from Wiley.

where $\Delta\mathbf{\Lambda}$ in eqs 42 and 43 collects the differences between experimental and calculated normal-mode frequencies. This leads to the true diagonal force constant matrix $\mathbf{K}'$ within the harmonic framework provided by the normal mode vectors $\mathbf{d}_\mu$. The adiabatic mode analysis can then be performed in the same way as it is for the calculated frequencies. An example illustrating this procedure can be found in ref 110 for the water dimer. If there are less than N_{vib} measured normal-mode frequencies available, which is often the case, calculated normal-mode frequencies can be used to complement the set.[110−112]

Adiabatic Connection Scheme (ACS). An important milestone for the local mode theory was the proof that there exists a 1:1 relationship between a complete set of nonredundant local modes and the normal modes via an *adiabatic connection scheme*, allowing a smooth transition from local to normal modes.[102] With the help of the inverse of $(\mathbf{F}^{\mathbf{q}})^{-1}$ the so-called *compliance matrix* $\mathbf{\Gamma}$[117] the vibrational eigenvalue eq 8 can be expressed as

$$\mathbf{\Gamma}^{-1}\mathbf{D} = \mathbf{G}^{-1}\mathbf{D}\mathbf{\Lambda} \tag{44}$$

$$\mathbf{GR} = \mathbf{\Gamma R}\mathbf{\Lambda} \tag{45}$$

A new eigenvector matrix $\mathbf{R}$ is given by

$$\mathbf{R} = \mathbf{\Gamma}^{-1}\mathbf{D} = \mathbf{F}^{\mathbf{q}}\mathbf{D} = (\mathbf{D}^{-1})^{\dagger}\mathbf{K} \tag{46}$$

Zou and co-workers partitioned the matrices $\mathbf{\Gamma}$ and $\mathbf{G}$ into diagonal ($\mathbf{\Gamma}_d$ and $\mathbf{G}_d$) and off-diagonal parts ($\mathbf{\Gamma}_{od}$ and $\mathbf{G}_{od}$):[102]

$$(\mathbf{G}_d + \lambda\mathbf{G}_{od})\mathbf{R}_\lambda = (\mathbf{\Gamma}_d + \lambda\mathbf{\Gamma}_{od})\mathbf{R}_\lambda\mathbf{\Lambda}_\lambda \tag{47}$$

The perturbation parameter λ in eq 47 slowly converts the local vibrational modes, ($\lambda = 0$) adiabatically into their corresponding normal mode counterparts, ($\lambda = 1$) by slowly switching on $\mathbf{\Gamma}_{od}$ and $\mathbf{G}_{od}$, i.e., by switching on the masses and in this way activating the mass-coupling. This one-to-one transformation between local and normal vibrational modes forms the fundamental proof for the decomposition of normal modes into local mode contributions opening new avenues for a comprehensive analysis of vibrational spectra.

Characterization of Normal Modes (CNM). In addition to local mode force constants and local mode frequencies, the local mode analysis has led to a new way of analyzing vibrational spectra. The CNM procedure decomposes each normal vibrational mode $\mathbf{l}_\mu$ into local mode contributions for a nonredundant set of N_{vib} local vibrational modes $\mathbf{a}_\mathbf{n}$ by calculating the overlap between each local mode vector $\mathbf{a}_n^x$ with this normal mode vector, $\mathbf{l}_\mu$ as $S_{n\mu}$ according to eq 48[92−94]

$$S_{n\mu} = \frac{(\mathbf{a}_n^x, \mathbf{l}_\mu)^2}{(\mathbf{a}_n^x, \mathbf{a}_n^x)(\mathbf{l}_\mu, \mathbf{l}_\mu)} \tag{48}$$

where $(\mathbf{a}, \mathbf{b})$ is the scalar product of two vectors $\mathbf{a}$ and $\mathbf{b}$ including a metric

$$(\mathbf{a}, \mathbf{b}) = \sum_{i,j} a_i O_{ij} b_j \tag{49}$$

O_{ij} is an element of the metric matrix $\mathbf{O}$. We generally use the force constant matrix $\mathbf{F}^x$ as metric, namely, $\mathbf{O} = \mathbf{F}^x$, to include the influence of the electronic structure. As derived by Konkoli and Cremer[92] the contribution of local mode $\mathbf{a}_n$ to the normal mode $\mathbf{l}_\mu$ is given by

$$C_{n\mu} = \frac{S_{n\mu}}{\sum_m^{N_{\text{vib}}} S_{m\mu}} \tag{50}$$

i.e., a completely localized normal mode $\mathbf{l}_\mu$ has a $C_{n\mu}$ value of 1 (corresponding to 100% if $C_{n\mu}$ is given as percentage). In essence, the CNM procedure complements the ACS analysis with a nonadiabatic picture, i.e., a snapshot of the normal modes expressed in terms of the local mode contributions. As an illustration, the ACS and CNM plots (Figure 1a and 1b, respectively) of methylthiocyanate, a prototype for popular CN vibrational Stark effect (VSE) probes[118] are shown, clearly revealing that the CN probe bond in CH_3SCN is strongly localized, which is the prerequisite for a perfect VSE probe.[119−121]

It has to be noted that whereas LMA properties can be calculated for a restricted number of local mode parameters, both ACS and CMN require a complete nonredundant set of N_{vib} local mode parameters. There are different possibilities to define a nonredundant set of local mode parameters, often being guided by chemical intuition. Work is in progress to develop an automatic procedure which narrows down the number of possibilities by minimizing the coupling frequencies between local and normal mode,[102] complemented with thermodynamic information. In addition, we are exploring the possibility to derive the physically meaningful sets guided by Lagrangians that

https://doi.org/10.1021/acs.jpca.2c05962
J. Phys. Chem. A 2022, 126, 8781−8798

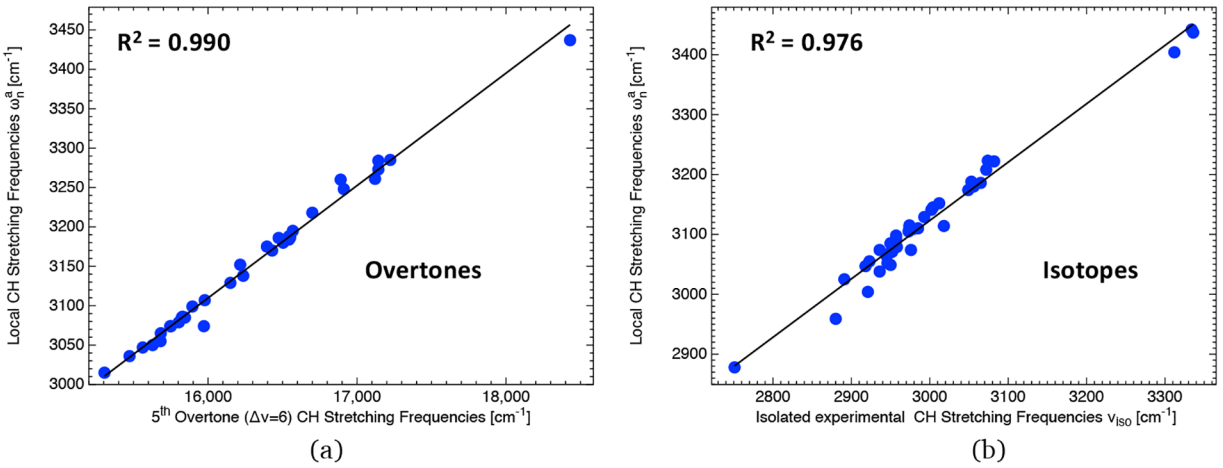

Figure 2. (a) Local mode stretching frequencies versus fifth overtone CH stretching frequencies (experimental data was taken from Table 4.3 of ref 105). (b) Local mode versus isolated CH stretching frequencies derived from isotope substitution. from Table 1 of ref 112. Reprinted with permission from ref 89. Copyright 2020 from Wiley.

lead to the same equations of motion for the sets under consideration.[125]

As a closing remark of this section, our local CH vibrational mode frequencies correlate well with experimentally derived local modes from overtone spectroscopy[105] and with local modes derived via isotope substitution (see Figure 2);[112] details are given in ref 89. However, the use of overtone spectroscopy as a means of obtaining local mode information is mostly limited to terminal bonds, difficult for complex systems such as proteins.[50,126−128] Extensive use of isotope effects to other than XH bonds[129] is difficult regarding the huge experimental effort and the fact that isotopes which considerably increase the atomic masses are not available for most of the atoms,[130] and therefore is mostly applied in specific cases, such as atomic-scale vibrational spectroscopy.[131] In summary, our approach offers a simpler and more straightforward way to derive localized vibrations compared to the complex route via overtone spectroscopy and/or isotope spectroscopy. The local vibrational mode software LModeA[132] has interfaces for about 20 popular quantum chemistry programs. The package, including source code, user manual, and tutorial, can be obtained on request free of charge from the authors, see Supporting Information for a more detailed description.

■ RESULTS AND DISCUSSION

LMA has advanced over the past years as a powerful bond strength descriptor accounting for both covalent bonds and noncovalent interactions stretching from hydrogen bonds, halogen bonds to tetrel bonds and π-whole interactions. Some recent examples include refs 133−135. Different molecular environments were considered such as systems in solution[136] or in proteins.[137] Another focus has been metal−ligand bonding, which led to a new metal−ligand electronic parameter (MLEP), i.e., the local metal−ligand force constant as a quantitative measure of the metal−ligand bond strength replacing the more qualitative Tolman electronic parameter (TEP), which assesses the metal−ligand bond strength in carbonyl complexes indirectly via the normal CO stretching frequency.[138−140] Going beyond LMA's use as bond strength descriptor, a new aromaticity index was defined,[141−143] new measures for chemical similarity,[144,145] molecular acidity,[146] and chiral discrimination[147] were established. LMA was paired up with the Cremer−Pople ring puckering analysis[99] to shed new light into the conformation of deoxyribonucleosides,[148] and the concept of σ- and π-holes was translated into vibrational spectroscopy,[134] just to name a few. Recently, a whole new scope of chemical systems was unlocked with the extension of LMA to periodic systems and crystals.[149,150] In addition, CNM studies have provided a new way to analyze vibrational spectra as applied to provide a measure for assessing the quality of Stark-effect probes[121] the community has been looking for. In the following, some representative LMA applications are highlighted (for a comprehensive overview of LMA showing the breadth of application possibilities, the reader is referred to ref 89 and references therein). At the end of this section recent applications of LMA by other groups are reported.

Metal−Ligand Bonding in Heme Proteins. The quantification of metal−ligand bonding in proteins is of paramount importance for a deeper understanding of biochemical processes.[151] As an example, heme proteins such as myoglobin (Mb)[152] and neuroglobin (Ngb),[153,154] both members of the globin superfamily of proteins,[155,156] share a comparable active site with a prosthetic heme group consisting of a protoporphyrin ring with a central iron core, which is attached to the protein backbone via the proximal histidine. Signaling ligands L such as CO, NO, O_2, H_2S coordinate to the Fe on the opposite site of the porphyrin ring interacting with the distal histidine. Their key role is to cause conformational changes of the protein, resulting in diverse enzymatic activities.[155−157] In higher doses, ligands such as CO or H_2S can lead to poisoning[158,159] or to oxidative stress.[160] Therefore, it is imperative to learn more about FeL and L···H binding in these enzymes. Vibrational spectroscopy studies, including difference spectroscopy,[161] Far-IR and THz domain spectroscopy,[162] resonance Raman,[163−165] and time-resolved resonance Raman,[166] complemented with computational investigations[153,167] have suggested that the biological functions of these proteins are related to the strength of the FeL bond, without being able to quantify these effects. In three recent studies applying LMA and a hybrid QM/MM methodology,[168] we could for the first time (i) quantify the suggested inverse correlation between the CO and FeC bond strength[165] and the special role of CO···H bonding in Mb[137] and (ii) successfully clarify the binding mode of azanone (HNO) to the heme group

https://doi.org/10.1021/acs.jpca.2c05962
J. Phys. Chem. A 2022, 126, 8781−8798

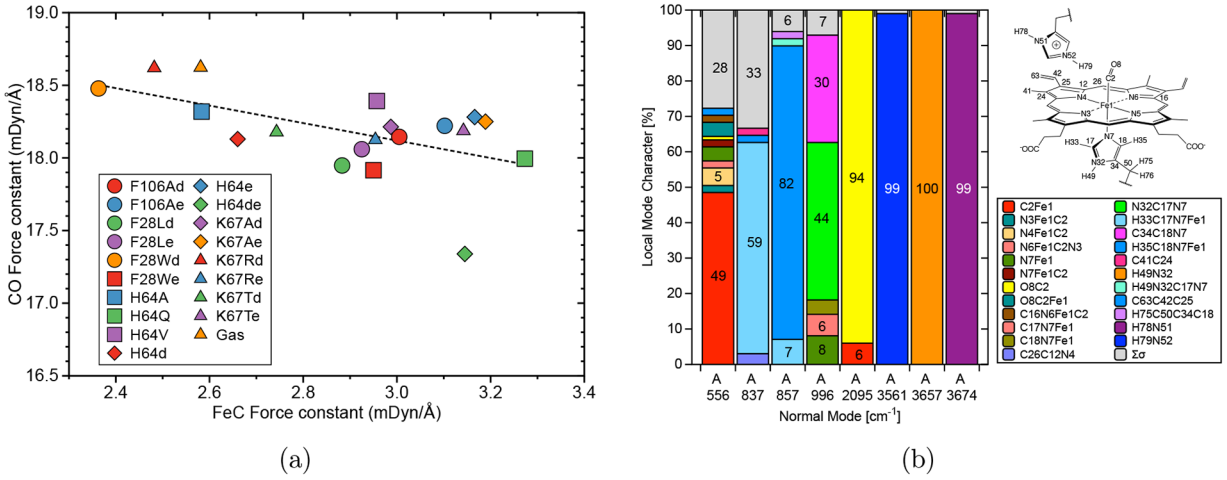

Figure 3. (a) Relation between the CO local mode force constant and the FeC local mode force constant for the wild type NgbCO and its protein mutations. (b) Decomposition of the selected normal modes into local mode components for the protonated distal histidine of NgbCO (H64$\delta\epsilon$). $\Sigma\sigma$ comprises the summation of all of the σ local mode contributions below the threshold of 1%; details of the calculations can be found in the in the Supporting Information.

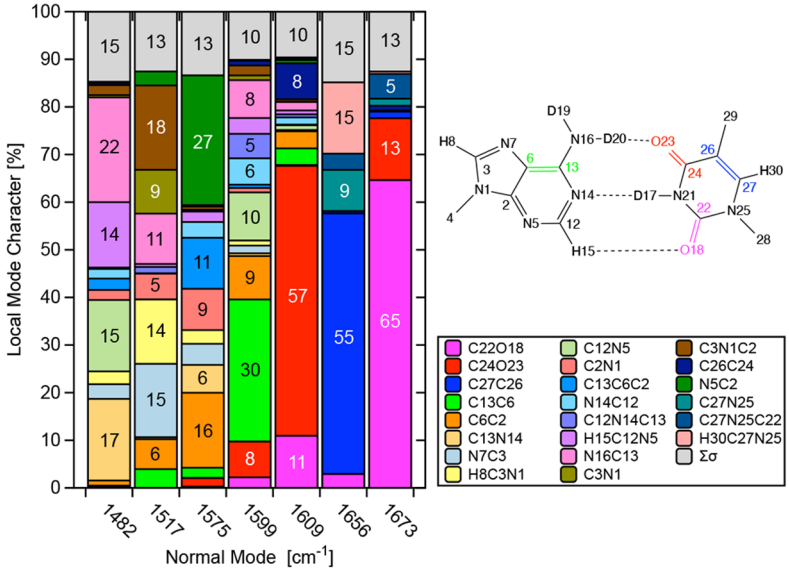

Figure 4. CNM plot of the characteristic vibrational region of deuterated 9-methyladenine:1-methylthymine base pair (AT) at the ωB97X-D(PCM)/aug-cc-pVTZ level of theory in the cavity within the water dielectric medium.[122−124,180] Bonds suggested for base-pair coupling in the literature are colored in the Chemdraw sketch (see text for details). Normal mode frequencies are scaled for anharmonicity effects by a factor of 0.9614. $\Sigma\sigma$ comprises the summation of all of the σ local mode contributions below the threshold of 5%.

of Mb,[117] a long debated question.[157] Utilizing the same computational protocol as applied in our MbCO study[137] we investigated CO bonding in hexacoordinate (CO ligated to Fe) and penta-coordinate (CO dissociated from the heme group but trapped in the active site) scenarios for the wild type NgbCO and nine known protein mutations, see Supporting Information for details.[169] In contrast to MbCO we found a less pronounced correlation between the CO and FeC bond strength, see Figure 3a. Further interesting details are revealed by the CNM analysis shown in Figure 3b. The normal CO stretching mode at 2095 cm^{-1} is 94% localized, there is no particular hydrogen bond interaction with the distal histidine (NH stretching at 3657 cm^{-1} is 100% localized), whereas the Fe−C bond (556 cm^{-1}) strongly couples with porphyrin and proximal histidine motions. These results qualify the CO bond as convenient probe to monitor changes of the electronic effects during protein modification providing valuable insights for the fine-tuning of existing and the design of new neuroglobin models with specific FeC and CO bond strengths.

Disentanglement of DNA Vibrational Modes. Linear and nonlinear vibrational spectroscopies have been of particular interest to monitor changes in the secondary structure of DNA.[170−177] Nevertheless, categorical structural assignment of the characteristic normal vibrational modes within the frequency range of 1500−1800 cm^{-1}, which is the fingerprint region of in-plane base vibrations, is hindered by spectral congestion.[170,177,178] Not only does spectral congestion pose a conundrum for nucleic acids, but for polyatomic molecules as a whole, as a result of the very nature of normal vibrational modes.[101] High delocalization and, consequently, different types of interactions between functional groups (vibrational coupling) make it hard to determine specific bond contributions as spectral

https://doi.org/10.1021/acs.jpca.2c05962
J. Phys. Chem. A 2022, 126, 8781−8798

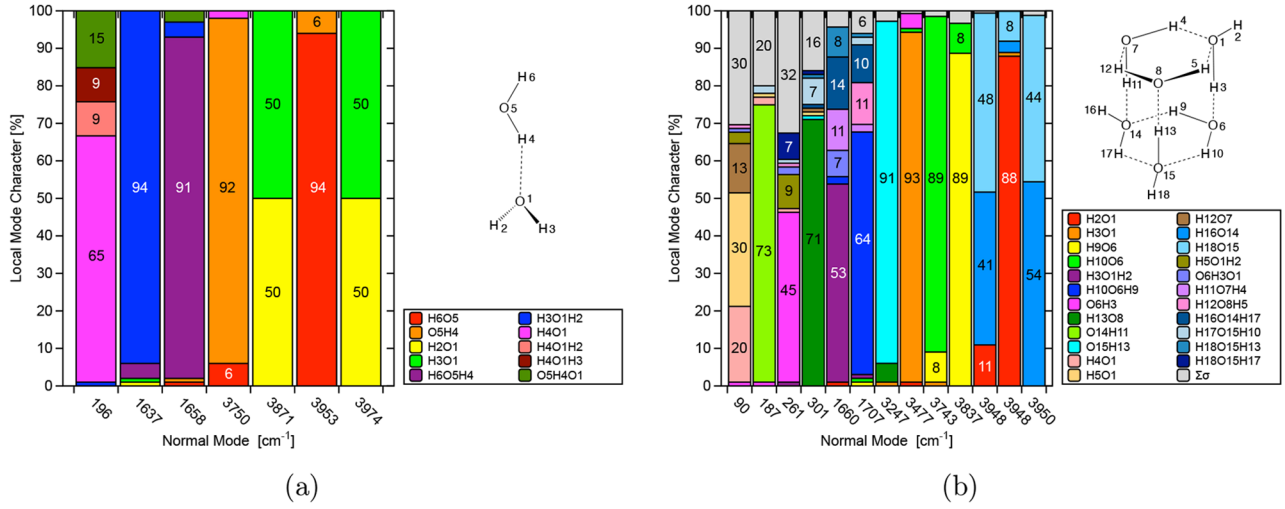

Figure 5. CNM plots of (a) the water dimer (C_s) and (b) the water prism hexamer (C_1). Calculations were performed at the ωB97X-D/aug-cc-pVTZ level of theory. The vibrational space in both cases was chosen so as to reveal the differences upon clustering, as well as the strongest and weakest hydrogen bonds and O−H covalent bonds in (b) (see text for details). Σσ comprises the summation of all of the σ local mode contributions below the threshold of 6%.

signatures of polyatomic molecules of interest.[170,179] LMA offers a helping hand to detangle the congested information.

2D IR derived normal-mode frequencies suggest that specific CC and CO stretching vibrations in adenine (A), guanine (G), cytosine (C), and thymine (T) are prone to base pair coupling in the fingerprint region.[171,173−175,177,178] Figure 4 shows the CNM analysis for the A:T base pair, which clearly confirms and quantifies the experimentally based proposal. The normal mode associated with the fingerprint vibration at 1599 cm^{-1} has a 30% contribution of the CC bond (green color) of adenine and smaller contributions from the CC and the two CO bonds (orange, blue, and pink color) of thymine as suggested. The normal mode associated with the fingerprint vibration at 1656 cm^{-1} contains 55% CC coupling (blue color, Figure 4) and the fingerprint vibration at 1673 cm^{-1} contains 65% and 13% CO coupling (blue and pink color, respectively, see Figure 4) of thymine. These results show how LMA and in particular CNM can considerably increase our current understanding of the secondary structure of DNA.

Hydrogen Bonding in Water Clusters and Ice. A common theme in determining the vibrational spectroscopy of water is unraveling site-specific interactions in water clusters, namely in characterizing the free and bound O−H stretches. Using linear spectroscopy, such as FTIR and Raman, can reveal essential information about hydrogen bond strengths and the local environment of water through the OH stretching mode frequency; however, these spectra often suffer from spectral congestion and band broadening.[181,182] Beyond purely vibrational spectroscopy, vibrational SFG has recently been used in visualizing the extent of interfacial water and probing water−surface interactions.[24,183,184] This technique improves upon pure IR measurements by distinct electronic excitations that suggest molecular locality and directionality in addition to characteristic vibrational modes. A special case of SFG is Second Harmonic Generation (SHG) spectra where the visible and IR excitation frequencies are identical; recent studies emphasizing second order nonlinear susceptibility measured in SHG have diminished some issues researchers have experienced in modeling more distinct features in charged interfaces and water−silica interfaces,[185−187] including acceptor−donor, acceptor−donor−donor (ADD), acceptor−acceptor−donor (AAD), as the main examples.[188] The AAD class is characterized by a free OH group while the ADD class is composed of exclusively bound OH groups. Many geometries can be achieved by mixing classes of these water models that present varying degrees of internal hydrogen bonding, which these demonstrate useful structural properties for researchers.[189] Recent computational advances include the calculation of vibrational spectra of isolated molecules in perdeuterated cages, which allow for the isolation of specific O−H stretching modes depending on the site of addition.[190] Other methods have focused on analyzing local behavior of cold clusters to reduce the extent of congestion and band-broadening seen in observing characteristic transitions of the O−H stretch in the 3000−3700 cm^{-1} region.[188,191] The chemistry of protonated water clusters has been explored using VCI-VSCF, in particular to probe local structural defects involved in site-specific protonation across the hydrogen bonding network, showing a good match for experimental measurements of protonated water clusters and better account for anharmonicity via AIMD data.[126,192,193] In this scenario, LMA provides the perfect complementary tool to shed more light into the multiplex structures of water by quantifying the strength of individual O−H and hydrogen bonds in these complex systems. Recent calculations with LMA of water clusters demonstrate a push−pull effect[194] contributing to the relative O−H bond strengths seen in the prism hexamer when compared to the water dimer. Figure 5 shows the characterization of normal modes for the water dimer (C_s)[110] compared against the water prism hexamer (C_1).[194] The vibrational space selected for the water dimer can be contrasted with that of the water prism (the same colors represent the local vibrational modes mirrored between the two systems). It should be noted that the normal vibrational mode at 196 cm^{-1} for the water dimer has 65% of H4O1 character, which represents the only hydrogen bond. The remaining part of the vibrational space is related to bond and angle local vibrational modes. The region 3247−3837 cm^{-1}, while noticeably blue-shifted, matches with the expected region of the bound O−H stretch in 3000−3600 cm^{-1},[188] and the local modes within this region comprise the major character for the associated normal modes. The region

https://doi.org/10.1021/acs.jpca.2c05962
J. Phys. Chem. A 2022, 126, 8781−8798

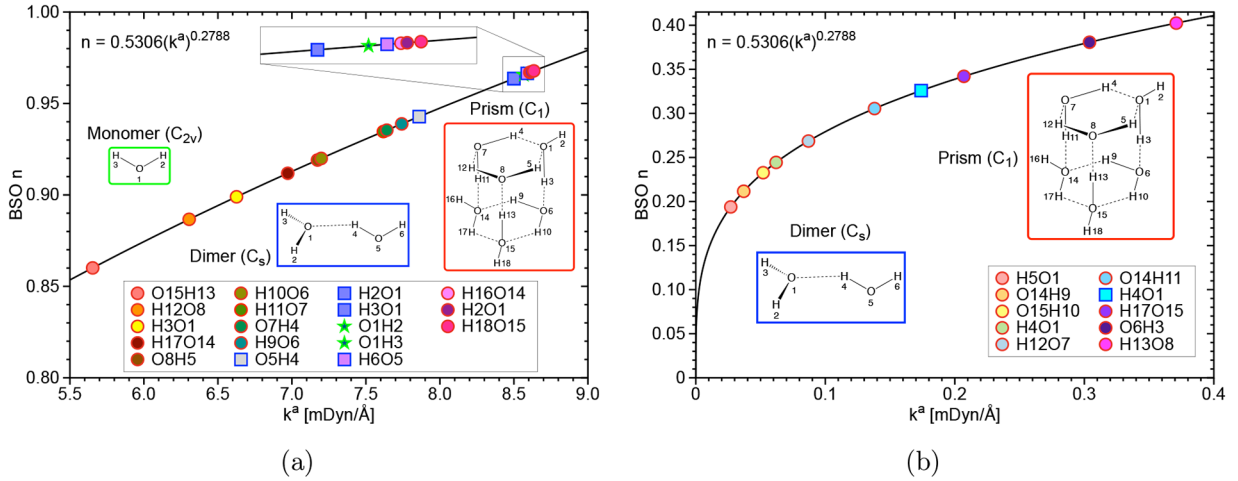

Figure 6. Relative BSO n versus k^a for (a) O−H covalent bonds of the water monomer (C_{2v}), the water dimer (C_s), and the water prism hexamer (C_1) and (b) hydrogen bonds of the water dimer (C_s) and the water prism hexamer (C_1). Calculations were performed at the ωB97X-D/aug-cc-pVTZ level of theory.[122−124]

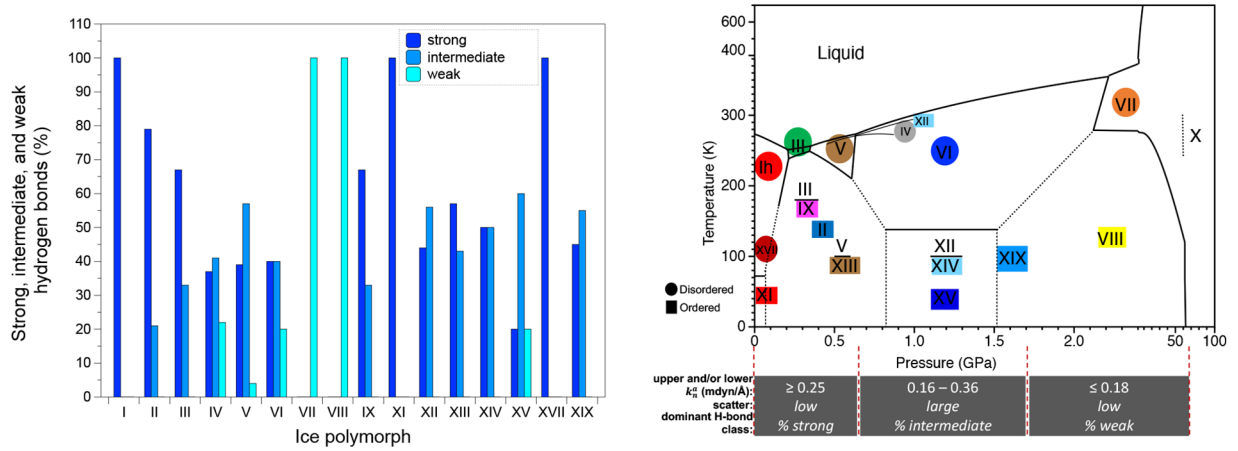

Figure 7. (a) Percentage of strong, intermediate, and weak hydrogen bond classes within each ice polymorph, represented by differently colored bars. Classification according to lk_n^a values: ≥0.250 mdyn/Å strong, 0.249−0.177 mdyn/Å intermediate, and ≤0.176 mdyn/Å weak. (b) Hydrogen bond strength variation across the water−ice phase diagram. Gray bars spanning three pressure regions (0−0.7, 0.7−1.6, 1.6−50 GPa). Circles and squares distinguish between disordered and ordered ices respectively, and colors for indicating different ices. Computational details are given in ref 150. Reprinted with permission from ref 150. Copyright 2022 from the American Chemical Society.

3948−3950 cm^{-1} also matches the expectation for the free O−H stretch around 3700 cm^{-1},[191] with some overlap in the normal mode 3948 cm^{-1} due to the degeneracy of the set of local modes selected. For the water prism, the decomposition of normal vibrational modes was intended to show, besides the comparison with the dimer, the composition in terms of the local vibrational modes encoding information about the strongest and weakest O−H covalent bonds and hydrogen bonds, as revealed by Figure 6a and 6b, respectively. Figure 6 compares k^a values in terms of a relative bond strength order (BSO) n based on the HF bond of FH with BSO n of 1 and the HF bond of the $[F−H−F]^{-1}$ anion with BSO n of 0.5. In accounting for the relative length of the interaction spanned by the hydrogen bonding shown in the hexamer compared to the dimer, these interactions appear to benefit from neighboring hydrogen bonding partners polarizing individual hydrogen bonds to increase the overall strength of the individual O−H stretches as shown by the relative force constants (k^a). This phenomenon that has been described in a prior study as the push−pull effect of hydrogen bonding in clusters.[194] Figure 6 substantiates the patterns viewed in Figure 5 as the free O−H stretches are shown to be the strongest interactions where the bonded O−H stretches are much weaker.

We have also applied local mode force constants derived from periodic local vibrational modes[149] to quantify the intrinsic hydrogen bond strength of 16 ice polymorphs, ices II$_h$, II, III, IV, V, VI, VII, VIII, IX, XI, XII, XIII, XIV, XV, XVII, and XIX, that are stable under ambient to elevated pressures.[150] Analyzing ca. 2000 different hydrogen bonds in these polymorphs we found that I$_h$ (the most frequently occurring hexagonal form of ice on the Earth), XI, and XVII ices have the strongest hydrogen bonds, on the opposite side of the spectrum ices VII and VIII (existing in the Earth interior) have the weakest H-bonds whereas Ices II, III, IX, XII, XIII, XIV and XIX have strong and intermediate hydrogen bonds and ices IV, V, VI, and XV have all three types, as depicted in Figure 7a. Relating our results to the currently accepted water-ice diagram[195] (see Figure 7b) reveals that ices

https://doi.org/10.1021/acs.jpca.2c05962
J. Phys. Chem. A 2022, 126, 8781−8798

in the 0−0.7 GPa region are dominated by strong hydrogen bonds; ices in the central region (0.7−1.6 GPa) have a high percentage of intermediate hydrogen bonds whereas ices in the high-pressure region (up to 50 GPa) are mostly comprised of weak hydrogen bonds. Based on these findings we suggest using local mode force constants as a tool to predict at what pressure a new ice form will most likely be stable, guiding complex experiments aimed at verifying predicted ice forms; currently more than 50.[196]

Use of LMA by Other Groups. LMA has begun to be used by other research groups for a number of different topics. For example, the Gatto group[197] has utilized LMA to decompose normal modes into local modes (via CNM procedure) of heterogeneous atoms in a binuclear copper(II) complex with a hydrazone ligand. They were able to determine the information that is hidden in the vibrational normal modes and compare the local vibrational frequencies from different DFT functionals with their experimental spectra results. Local force constants were recently used by Zou et al.[198] to study the properties of copernicium fluorides, where they were able to qualitatively show the trend of Cn−F bond lengths and force constants with respect to generalized Mayer's Bond Order of Cn−F. This trend describes that there is a single bond in CnF_2, CnF_4, CnF_6, and half a bond in CnF. Morrison et al.[199] studied bond strengths by using LMA for 31 CHNO-containing molecules. They were able to observe an exponential relationship between the local force constants and the bond length of seven different CHNO-covalent bonding types, where the strongest bond was the shorter bond length. Kabir and co-workers[200] used LMA to describe the hydrogen bonding profile of the isoalloxazine ring in the lumiflavin molecule. Bond lengths, local force constants, and bond strength orders BSO *n* were calculated for all bonds in the lumiflavin molecule, and it was quantitatively determined the carbonyl carbons exhibited the greatest sensitivity to hydrogen bonding in the flavin scaffold. To study the strengths of various internal hydrogen bonding types, Trindle and collaborators[201] used LMA to rank the relative bond strengths with the relative stretching force constants. With the power relationship between the local force constant and the density at the bond critical point, they were able to order the bond strength as such: strongest O−H···O═C > N−H···O═C > O−H···N, intermediate N−H···O═C ≥ N−H···O ≈ C−H···O═C, and weakest C−H···N > C−H···O. Gargano and associates[202] recently used LMA as a validation metric for their calculations concerning amino radical-noble gas adducts. They concluded that the local force constants they observed for their complexes fell inline with the lowest calculated dissociation energies for the bonding interactions, and deduced these models provided congruent characterizations for the model chemistry. Burger and his group[203] were able to confirm the weak interactions between binuclear copper(I) pyridine diimine centers when comparing the local force constants to the Mayer bond order and Wiberg and Fuzzy Cu−Cu bond orders. They also recently applied LMA in a study on the rare cleavage of an aromatic C−C bond in ferrocene by insertion of an iridium nitrido nitrogen atom. Wilcox and collaborators successfully used LMA force constants to study weak interactions of 2-coordinate iodine(I) silver(I) with nucleophilic iodonium in solution.[204] Klüfers et al. recently reported the first Ru-complex, the dinitrosylruthenium [$Ru(NO)_2(PPh_3)_2$, which can serve as a unique synchronous photoswitching device via a transformation of the double-linear to a double-bent $Ru(NO)_2$ core under nitrosyl charge conservation.[205] They used LMA to clarify that this trans-formation in not a [2 × 2] electron redox process, i.e., the observed redshift of the N−O stretching frequency occurs despite the lack of an additional electron-density transfer with both, the Ru−N and the N−O bonds becoming weaker upon bending.

SUMMARY AND CONCLUDING REMARKS

In this Feature Article, an overview of the current status of the local mode theory is given showing how it can complement and bridge current experimental and theoretical efforts to interpret the constantly increasing wealth of vibrational spectroscopy data collected. Special features of the local mode theory include

- Derivation of local modes from mass-decoupled Euler−Lagrange equations curing the problem that normal vibrational mode modes are generally delocalized in polyatomic systems concealing specific information.
- A 1:1 relationship between the normal vibrational modes and a complete, nonredundant set of local vibrational modes via an adiabatic connection scheme (ACS). This relationship forms the basis for the decomposition of each normal mode into local mode contributions (CNM) which has already led to a new way of analyzing vibrational spectra.
- Local mode stretching force constants that are directly related to the intrinsic strength of a bond and/or weak interaction and, therefore provide a unique measure of bond strength based on vibrational spectroscopy across chemical bonds and weak chemical interactions.
- The local mode analysis can also be applied to experimentally derived vibrational frequencies within the framework of the harmonic approximation of the potential energy, and in this way covering anharmonicity effects and model chemistry dependencies at low cost.
- Local mode properties of molecules and periodic systems can be directly compared.

Three current focus points of the local mode analysis are reported, demonstrating how the local mode analysis extracts important information hidden in vibrational spectroscopy data supporting current experiments:

- Metal−ligand bonding in heme protein complexes quantifying the inverse relationship between the FeC and CO bond strengths in MbCO and NgbCO complexes.
- Disentanglement of DNA vibrational modes and a quantitative validation of methyladenine and methylthymine base pairing.
- Hydrogen bonding in water clusters and ice and a new description illustrating the induced polarization from periphery molecules in the cluster.
- In addition, the use of the local mode analysis by other research groups was reviewed.

Current and planned applied work in progress include the application of LMA's unique features to declutter vibrational spectra, such as assisting isotope-edited IR spectroscopy pinpointing specific bonds of interest in the IR spectrum of DNA, which is hampered by the large number of overlapping carbonyl signals;[170] monitoring oxidation state changes in photoactive enzymes via changes in LMA properties in support of, e.g., protein film electrochemistry;[206] combining LMA with the group's unified reaction valley approach (URVA)[207] to model properties of artificial metalloenzymes and their catalytic mechanisms;[208,209] applying LMA's potential in the emerging

https://doi.org/10.1021/acs.jpca.2c05962
J. Phys. Chem. A 2022, 126, 8781−8798

field of covalent binder drugs,[210] which strongly depends on reliable, quantitative bond strength descriptors;[139,211] and on the other end of the spectrum, investigating a large number of reported ionic crystals with the far-reaching goal to compile a database with individual local mode force constants, serving as a basis for comprehensive studies on how important physico-chemical properties, e.g., electrical conductivity and optical properties of these crystals are related to the individual bond strengths in these materials.

The overarching goal of this Feature Article is to present a new tool to the computational community which can be easily applied after a quantum chemical calculation of vibrational frequencies, leading to a wealth of additional electronic structure information, complementing experimental and theoretical efforts aimed exploring the structure of molecules in gas phase, liquid and protein environments, and/or in crystals. Our vision is that in the future, the local mode analysis will be routinely applied within the community and that this article serves as an incubator for future collaborations between experiment and theory.

■ ASSOCIATED CONTENT

Supporting Information

The Supporting Information is available free of charge at https://pubs.acs.org/doi/10.1021/acs.jpca.2c05962.

Details about the NgbCO study; NgbCO complexes investigated; QM/MM computational details for the NgbCO example; Extraction of QM part for CNM analysis; and LModeA software (PDF)

■ AUTHOR INFORMATION

Corresponding Author

Elfi Kraka − *Computational and Theoretical Chemistry Group (CATCO), Department of Chemistry, Southern Methodist University, Dallas, Texas 75275-0314, United States;* orcid.org/0000-0002-9658-5626; Email: ekraka@gmail.com

Authors

Mateus Quintano − *Computational and Theoretical Chemistry Group (CATCO), Department of Chemistry, Southern Methodist University, Dallas, Texas 75275-0314, United States*

Hunter W. La Force − *Computational and Theoretical Chemistry Group (CATCO), Department of Chemistry, Southern Methodist University, Dallas, Texas 75275-0314, United States*

Juliana J. Antonio − *Computational and Theoretical Chemistry Group (CATCO), Department of Chemistry, Southern Methodist University, Dallas, Texas 75275-0314, United States;* orcid.org/0000-0002-0358-9274

Marek Freindorf − *Computational and Theoretical Chemistry Group (CATCO), Department of Chemistry, Southern Methodist University, Dallas, Texas 75275-0314, United States*

Complete contact information is available at: https://pubs.acs.org/10.1021/acs.jpca.2c05962

Author Contributions

‡Contributed equally to this work.

Notes

The authors declare no competing financial interest.

Biographies

Elfi Kraka is Full Professor and Chair of the Department of Chemistry at Southern Methodist University, Dallas, Texas, USA, since 2009, and since 2017, has been the head of the Computational and Theoretical Chemistry group (CATCO). She received her Dr. rer. nat. in Theoretical Chemistry at the University of Cologne, Germany with summa cum laude. CATCO's research mission is to develop modern quantum chemical tools and to apply these tools to solve pending problems in chemistry, biology, materials science, and beyond. Current research topics stretch from catalysis, vibrational spectroscopy to machine learning supported computer assisted drug design. She has published more than 250 peer-refereed articles and presented her research at about 150 international conferences. She is a member of the Scientific Board of the World Association of Theoretical and Computational Chemists (WATOC) and serves on several the Editorial Boards.

Mateus Quintano received both his B.S. (2018) and M.S. (2020) in Chemistry from the Federal University of Minas Gerais, Brazil. He is currently a third year Ph.D. student in the CATCO research group at Southern Methodist University. His career path has been marked by research interests focused on vibrational spectroscopy, statistical thermodynamics, and mathematical methods. He is recipient of a SMU CSE Ph.D. fellowship.

https://doi.org/10.1021/acs.jpca.2c05962
J. Phys. Chem. A 2022, 126, 8781−8798

Hunter W. La Force is a second-year graduate student in the CATCO research group at Southern Methodist University. His research interests range from modeling protein conformational dynamics using ML-aided molecular dynamics to employing tools of quantum chemistry in solving problems related to Computer-Aided Drug-Design. La Force completed his undergraduate studies in 2021 at the University of Redlands in Redlands, California. He began his Ph.D. at Southern Methodist University in 2021 and joined the CATCO group in 2022. He is the recipient of a DSF Charitable Foundation Ph.D. fellowship.

Juliana J. Antonio attended the University of Texas at Rio Grande Valley where she received her B.Sc. with honors in chemistry. She is currently a first year Ph.D. student in the CATCO research group at Southern Methodist University. Her current research interests include QM/MM of organometallic proteins with vibrational local mode analysis and reaction mechanism profiles of various organometallic complexes. She is the recipient of an SMU Mustang Ph.D. fellowship.

Marek Freindorf graduated with MS and PhD (with honors) in Chemistry and minor in Physics from Jagiellonian University (Poland) in 1988. He was a faculty member in Chemistry Department of Jagellonian University until 2000 and worked as a postdoctoral research associate in University of Bonn (Germany), University at Buffalo NY (USA), and University of Louisville KY (USA). From 2011, he has held a Research Professor position in Chemistry Department of SMU (USA). He has authored about 60 papers involving theoretical molecular spectroscopy, computations of homogeneous catalysis with transition metals, and QM/MM calculations of DNA and protein active sites.

■ ACKNOWLEDGMENTS

This work was financially supported by the National Science Foundation (Grant CHE 2102461) and the DSF Charitable Foundation. We thank SMU's Center for Scientific Computing for providing generous computational resources and Vytor Oliveira for helpful comments and suggestions.

■ REFERENCES

(1) Ozaki, Y., Wójcik, M., Popp, J., Eds. *Molecular Spectroscopy: A Quantum Chemistry Approach*; Wiley, 2019; Vol. *1*.
(2) Ozaki, Y., Wójcik, M., Popp, J., Eds. *Molecular Spectroscopy: A Quantum Chemistry Approach*; Wiley, 2019; Vol. *2*.
(3) Koleżyński, A., Król, M., Eds. *Molecular Spectroscopy-Experiment and Theory*; Springer Cham, 2019.
(4) Wang, Y.; Chen, D. Application of Advanced Vibrational Spectroscopy in Revealing Critical Chemical Processes and Phenomena of Electrochemical Energy Storage and Conversion. *ACS Appl. Mater. Interfaces* **2022**, *14*, 23033−23055.
(5) Markelz, A. G.; Mittleman, D. M. Perspective on Terahertz Applications in Bioscience and Biotechnology. *ACS Photonics* **2022**, *9*, 1117−1126.
(6) Hess, C. New advances in using Raman spectroscopy for the characterization of catalysts and catalytic reactions. *Chem. Soc. Rev.* **2021**, *50*, 3519−3564.
(7) Ditler, E.; Luber, S. Vibrational spectroscopy by means of first-principles molecular dynamics simulations. *WIREs: Comput. Mol. Sci.* **2022**, *12*, No. e1605.
(8) Sathyanarayana, D.*Vibrational Spectroscopy: Theory and Applications*, 3rd ed.; New Age International: New Delhi, India, 2021.
(9) Beć, K. B.; Grabska, J.; Huck, C. W. Current and future research directions in computer-aided near-infrared spectroscopy: A perspective. *Spectrochim. Acta A Mol. Biomol. Spectrosc.* **2021**, *254*, 119625.
(10) Beć, K. B.; Grabska, J.; Hofer, T. S. In *Near-Infrared Spectroscopy: Theory, Spectral Analysis, Instrumentation, and Applications*; Ozaki, Y., Huck, C., Tsuchikawa, S., Engelsen, S. B., Eds.; Introduction to Quantum Vibrational Spectroscopy; Springer: Singapore, 2021; pp 83−110.
(11) Ozaki, Y.; Beć, K. B.; Morisawa, Y.; Yamamoto, S.; Tanabe, I.; Huck, C. W.; Hofer, T. S. Advances, challenges and perspectives of quantum chemical approaches in molecular spectroscopy of the condensed phase. *Chem. Soc. Rev.* **2021**, *50*, 10917−10954.
(12) Graefe, C. T.; Punihaole, D.; Harris, C. M.; Lynch, M. J.; Leighton, R.; Frontiera, R. R. Far-Field Super-Resolution Vibrational Spectroscopy. *Anal. Chem.* **2019**, *91*, 8723−8731.
(13) Cozzolino, D. Advantages, Opportunities, and Challenges of Vibrational Spectroscopy as Tool to Monitor Sustainable Food Systems. *Food Anal. Methods* **2022**, *15*, 1390−1396.
(14) Barone, V.; Alessandrini, S.; Biczysko, M.; Cheeseman, J. R.; Clary, D. C.; McCoy, A. B.; DiRisio, R. J.; Neese, F.; Melosso, M.; Puzzarini, C. Computational molecular spectroscopy. *Nat. Rev. Methods Primers* **2021**, *1*, 38.
(15) Sawaya, N. P. D.; Paesani, F.; Tabor, D. P. Near- and long-term quantum algorithmic approaches for vibrational spectroscopy. *Phys. Rev. A* **2021**, *104*, 062419.
(16) Jablonka, K. M.; Patiny, L.; Smit, B. Making Molecules Vibrate: Interactive Web Environment for the Teaching of Infrared Spectroscopy. *J. Chem. Educ.* **2022**, *99*, 561−569.

https://doi.org/10.1021/acs.jpca.2c05962
J. Phys. Chem. A 2022, 126, 8781−8798

(17) van Adrichem, K. E.; Jansen, T. L. C. AIM: A Mapping Program for Infrared Spectroscopy of Proteins. *J. Chem. Theory Comput.* **2022**, *18*, 3089−3098.
(18) Feng, C.-J.; Sinitskiy, A.; Pande, V.; Tokmakoff, A. Computational IR Spectroscopy of Insulin Dimer Structure and Conformational Heterogeneity. *J. Phys. Chem. B* **2021**, *125*, 4620−4633.
(19) Chrabaszcz, K.; Jasztal, A.; Smęda, M.; Zieliński, B.; Blat, A.; Diem, M.; Chlopicki, S.; Malek, K.; Marzec, K. M. Label-free FTIR spectroscopy detects and visualizes the early stage of pulmonary micrometastasis seeded from breast carcinoma. *Biochim. Biophys. Acta Mol. Basis Dis.* **2018**, *1864*, 3574−3584.
(20) Perez-Guaita, D.; Marzec, K. M.; Hudson, A.; Evans, C.; Chernenko, T.; Matthäus, C.; Miljkovic, M.; Diem, M.; Heraud, P.; Richards, J. S.; et al. Parasites under the Spotlight: Applications of Vibrational Spectroscopy to Malaria Research. *Chem. Rev.* **2018**, *118*, 5330−5358.
(21) Blat, A.; Dybas, J.; Chrabaszcz, K.; Bulat, K.; Jasztal, A.; Kaczmarska, M.; Pulyk, R.; Popiela, T.; Slowik, A.; Malek, K.; et al. FTIR, Raman and AFM characterization of the clinically valid biochemical parameters of the thrombi in acute ischemic stroke. *Sci. Rep.* **2019**, *9*, 15475.
(22) Guo, W.; Lu, T.; Gandhi, Z.; Chen, Z. Probing Orientations and Conformations of Peptides and Proteins at Buried Interfaces. *J. Phys. Chem. Lett.* **2021**, *12*, 10144−10155.
(23) Xu, R. J.; Blasiak, B.; Cho, M.; Layfield, J. P.; Londergan, C. H. A Direct, Quantitative Connection between Molecular Dynamics Simulations and Vibrational Probe Line Shapes. *J. Phys. Chem. Lett.* **2018**, *9*, 2560−2567.
(24) Tang, F.; Ohto, T.; Sun, S.; Rouxel, J. R.; Imoto, S.; Backus, E. H. G.; Mukamel, S.; Bonn, M.; Nagata, Y. Molecular Structure and Modeling of Water−Air and Ice−Air Interfaces Monitored by Sum-Frequency Generation. *Chem. Rev.* **2020**, *120*, 3633−3667.
(25) Hosseinpour, S.; Roeters, S. J.; Bonn, M.; Peukert, W.; Woutersen, S.; Weidner, T. Structure and Dynamics of Interfacial Peptides and Proteins from Vibrational Sum-Frequency Generation Spectroscopy. *Chem. Rev.* **2020**, *120*, 3420−3465.
(26) McDermott, M.; Vanselous, H.; Corcelli, S.; Petersen, P. DNA's Chiral Spine of Hydration. *ACS Cent. Sci.* **2017**, *3*, 708−714.
(27) Yan, E.; Fu, L.; Wang, Z.; Liu, W. Biological Macromolecules at Interfaces Probed by Chiral Vibrational Sum Frequency Generation Spectroscopy. *Chem. Rev.* **2014**, *114*, 8471−8498.
(28) Fu, L.; Liu, J.; Yan, E. Chiral Sum Frequency Generation Spectroscopy for Characterizing Protein Secondary Structures at Interfaces. *J. Am. Chem. Soc.* **2011**, *133*, 8094−8097.
(29) Wang, H.-L.; You, E.-M.; Panneerselvam, R.; Ding, S.-Y.; Tian, Z.-Q. Advances of surface-enhanced Raman and IR spectroscopies: from nano/microstructures to macro-optical design. *Light Sci. Appl.* **2021**, *10*, 161.
(30) Ma, J.; Yan, M.; Feng, G.; Ying, Y.; Chen, G.; Shao, Y.; She, Y.; Wang, M.; Sun, J.; Zheng, L.; Wang, J.; Abd El-Aty, M. An overview on molecular imprinted polymers combined with surface-enhanced Raman spectroscopy chemical sensors toward analytical applications. *Talanta* **2021**, *225*, 122031.
(31) Chaudhary, I.; Jackson, N.; Denning, D.; O'Neill, L.; Byrne, H. J. Contributions of vibrational spectroscopy to virology: A review. *Clin. Spectrosc.* **2022**, *4*, 100022.
(32) Bērziņš, K.; Fraser-Miller, S. J.; Gordon, K. C. Recent advances in low-frequency Raman spectroscopy for pharmaceutical applications. *Int. J. Pharm.* **2021**, *592*, 120034.
(33) Han, X. X.; Rodriguez, R. S.; Haynes, C. L.; Ozaki, Y.; Zhao, B. Surface-enhanced Raman Spectroscopy. *Nat. Rev. Methods Primers* **2021**, *1*, 87.
(34) Orlando, A.; Franceschini, F.; Muscas, C.; Pidkova, S.; Bartoli, M.; Rovere, M.; Tagliaferro, A. A Comprehensive Review on Raman Spectroscopy Applications. *Chemosensors* **2021**, *9*, 262.
(35) Cao, Y.; Sun, M. Tip-enhanced Raman spectroscopy. *Rev. Phys.* **2022**, *8*, 100067.
(36) Ma, H.; Han, X. X.; Zhao, B. Enhanced Raman spectroscopic analysis of protein post-translational modifications. *TrAC Trends Anal. Chem.* **2020**, *131*, 116019.
(37) Dybas, J.; Marzec, K. M.; Pacia, M. Z.; Kochan, K.; Czamara, K.; Chrabaszcz, K.; Staniszewska-Slezak, E.; Malek, K.; Baranska, M.; Kaczor, A. Raman spectroscopy as a sensitive probe of soft tissue composition − Imaging of cross-sections of various organs vs. single spectra of tissue homogenates. *TrAC Trends Anal. Chem.* **2016**, *85*, 117−127.
(38) Szczesny-Malysiak, E.; Dybas, J.; Blat, A.; Bulat, K.; Kus, K.; Kaczmarska, M.; Wajda, A.; Malek, K.; Chlopicki, S.; Marzec, K. M. Irreversible alterations in the hemoglobin structure affect oxygen binding in human packed red blood cells. *Biochim. Biophys. Acta Mol. Cell Res.* **2020**, *1867*, 118803.
(39) Dybas, J.; Alcicek, F. C.; Wajda, A.; Kaczmarska, M.; Zimna, A.; Bulat, K.; Blat, A.; Stepanenko, T.; Mohaissen, T.; Szczesny-Malysiak, E.; et al. Trends in biomedical analysis of red blood cells − Raman spectroscopy against other spectroscopic, microscopic and classical techniques. *TrAC Trends Anal. Chem.* **2022**, *146*, 116481.
(40) Sanchez, J. E.; Jaramillo, S. A.; Settles, E.; Velazquez Salazar, J. J.; Lehr, A.; Gonzalez, J.; Rodríguez Aranda, C.; Navarro-Contreras, H. R.; Raniere, M. O.; Harvey, M.; et al. Detection of SARS-CoV-2 and its S and N proteins using surface enhanced Raman spectroscopy. *RSC Adv.* **2021**, *11*, 25788−25794.
(41) Zhao, J.; Wang, Z.; Lan, J.; Khan, I.; Ye, X.; Wan, J.; Fei, Y.; Huang, S.; Li, S.; Kang, J. Recent advances and perspectives in photoinduced enhanced Raman spectroscopy. *Nanoscale* **2021**, *13*, 8707−8721.
(42) Bērziņš, K.; Sales, R.; Barnsley, J.; Walker, G.; Fraser-Miller, S.; Gordon, K. Low-wavenumber Raman spectral database of pharmaceutical excipients. *Vib. Spectrosc.* **2020**, *107*, 103021.
(43) Damle, V. H.; Aviv, H.; Tischler, Y. R. Identification of Enantiomers Using Low-Frequency Raman Spectroscopy. *Anal. Chem.* **2022**, *94*, 3188−3193.
(44) Lorenz-Fonfria, V. A. Infrared Difference Spectroscopy of Proteins: From Bands to Bonds. *Chem. Rev.* **2020**, *120*, 3466−3576.
(45) Buhrke, D.; Hildebrandt, P. Probing Structure and Reaction Dynamics of Proteins Using Time-Resolved Resonance Raman Spectroscopy. *Chem. Rev.* **2020**, *120*, 3577−3630.
(46) Banks, P.; Burgess, L.; Ruggiero, M. The necessity of periodic boundary conditions for the accurate calculation of crystalline terahertz spectra. *Phys. Chem. Chem. Phys.* **2021**, *23*, 20038−20051.
(47) Mitryukovskiy, S.; Vanpoucke, D.; Bai, Y.; Hannotte, T.; Lavancier, M.; Hourlier, D.; Roos, G.; Peretti, R. On the influence of water on THz vibrational spectral features of molecular crystals. *Phys. Chem. Chem. Phys.* **2022**, *24*, 6107−6125.
(48) Ishiyama, T.; Imamura, T.; Morita, A. Theoretical Studies of Structures and Vibrational Sum Frequency Generation Spectra at Aqueous Interfaces. *Chem. Rev.* **2014**, *114*, 8447−8470.
(49) Del Galdo, S.; Aschi, M.; Amadei, A. IR spectroscopy of condensed phase systems: Can the environment induce vibrational mode coupling? *Chem. Phys. Lett.* **2021**, *763*, 138168.
(50) Huso, J.; Ritter, J. R.; Bergman, L.; McCluskey, M. D. High Order Oxygen Local Vibrational Modes in ZnS1-xOx. *Phys. Status Solidi B* **2019**, *256*, 1800607.
(51) Kelley, J. D.; Leventhal, J. J.Normal Modes and Coordinates. In *Problems in Classical and Quantum Mechanics*; Springer, 2017; pp 95−117.
(52) Parks, H. L.; McGaughey, A. J. H.; Viswanathan, V. Uncertainty Quantification in First-Principles Predictions of Harmonic Vibrational Frequencies of Molecules and Molecular Complexes. *J. Phys. Chem. C* **2019**, *123*, 4072−4084.
(53) Hollingsworth, S. A.; Dror, R. O. Molecular Dynamics Simulation for All. *Neuron* **2018**, *99*, 1129−1143.
(54) Echenique, P.; Alonso, J. L. A mathematical and computational review of Hartree − Fock SCF methods in quantum chemistry. *Mol. Phys.* **2007**, *105*, 3057−3098.
(55) Verma, P.; Truhlar, D. G. Status and Challenges of Density Functional Theory. *Trends Chem.* **2020**, *2*, 302−318.

https://doi.org/10.1021/acs.jpca.2c05962
J. Phys. Chem. A 2022, 126, 8781−8798

(56) Mardirossian, N.; Head-Gordon, M. Thirty years of Density Functional Theory in Computational Chemistry: An Overview and Extensive Assessment of 200 Density Functionals. *Mol. Phys.* **2017**, *115*, 2315−2372.
(57) Zhang, I. Y.; Xu, X. On the top rung of Jacob's ladder of density functional theory: Toward resolving the dilemma of SIE and NCE. *WIREs: Comput. Mol. Sci.* **2021**, *11*, No. e1490.
(58) Sitkiewicz, S.; Zaleśny, R.; Ramos-Cordoba, E.; Luis, J.; Matito, E. How Reliable Are Modern Density Functional Approximations to Simulate Vibrational Spectroscopies? *J. Phys. Chem. Lett.* **2022**, *13*, 5963−5968.
(59) Lipparini, F.; Mennucci, B. Hybrid QM/classical models: Methodological advances and new applications. *Chem. Phys. Rev.* **2021**, *2*, 041303.
(60) Brehm, M.; Thomas, M.; Gehrke, S.; Kirchner, B. TRAVIS—A free analyzer for trajectories from molecular simulation. *J. Chem. Phys.* **2020**, *152*, 164105.
(61) Brehm, M.; Kirchner, B. TRAVIS - A Free Analyzer and Visualizer for Monte Carlo and Molecular Dynamics Trajectories. *J. Chem. Inf. Model* **2011**, *51*, 2007−2023.
(62) Mathias, G.; Ivanov, S. D.; Witt, A.; Baer, M. D.; Marx, D. Infrared Spectroscopy of Fluxional Molecules from (ab Initio) Molecular Dynamics: Resolving Large-Amplitude Motion, Multiple Conformations, and Permutational Symmetries. *J. Chem. Theory Comput.* **2012**, *8*, 224−234.
(63) Mathias, G.; Baer, M. D. Generalized Normal Coordinates for the Vibrational Analysis of Molecular Dynamics Simulations. *J. Chem. Theory Comput.* **2011**, *7*, 2028−2039.
(64) Teague, C. M.; Jordan, T. H.Partition Functions and Statistical Thermodynamics: Spreadsheet Activities To Promote Connections in Physical Chemistry. In *Engaging Students in Physical Chemistry*; American Chemical Society, 2018; pp 49−72. DOI: 10.1021/bk-2018-1279.ch004.
(65) Zapata Trujillo, J. C.; McKemmish, L. K. Meta-analysis of uniform scaling factors for harmonic frequency calculations. *WIREs: Comput. Mol. Sci.* **2022**, *12*, No. e1584.
(66) Morgan, W. J.; Matthews, D. A.; Ringholm, M.; Agarwal, J.; Gong, J. Z.; Ruud, K.; Allen, W. D.; Stanton, J. F.; Schaefer, H. F. Geometric Energy Derivatives at the Complete Basis Set Limit: Application to the Equilibrium Structure and Molecular Force Field of Formaldehyde. *J. Chem. Theory Comput.* **2018**, *14*, 1333−1350.
(67) Gong, J. Z.; Matthews, D. A.; Changala, P. B.; Stanton, J. F. Fourth-order vibrational perturbation theory with the Watson Hamiltonian: Report of working equations and preliminary results. *J. Chem. Phys.* **2018**, *149*, 114102.
(68) Paquet, E.; Viktor, H. L. Computational Methods for Ab Initio Molecular Dynamics. *Adv. Chem.* **2018**, 9839641.
(69) Manzhos, S.; Ihara, M. Computational vibrational spectroscopy of molecule−surface interactions: what is still difficult and what can be done about it. *Phys. Chem. Chem. Phys.* **2022**, *24*, 15158−15172.
(70) Fortenberry, R. C.; Lee, T. J. In *Computational Vibrational Spectroscopy for the Detection of Molecules in Space*; Dixon, D. A., Ed.; Annual Reports in Computational Chemistry; Elsevier, 2019; Vol. *15*, Chapter 6, pp 173−202.
(71) Gardner, M. B.; Westbrook, B. R.; Fortenberry, R. C.; Lee, T. J. Highly-accurate quartic force fields for the prediction of anharmonic rotational constants and fundamental vibrational frequencies. *Spectrochim. Acta A Mol. Biomol. Spectrosc.* **2021**, *248*, 119184.
(72) Baiz, C. R.; Błasiak, B.; Bredenbeck, J.; Cho, M.; Choi, J.-H.; Corcelli, S. A.; Dijkstra, A. G.; Feng, C.-J.; Garrett-Roe, S.; Ge, N.-H.; et al. Vibrational Spectroscopic Map, Vibrational Spectroscopy, and Intermolecular Interaction. *Chem. Rev.* **2020**, *120*, 7152−7218.
(73) Kananenka, A. A.; Yao, K.; Corcelli, S. A.; Skinner, J. L. Machine Learning for Vibrational Spectroscopic Maps. *J. Chem. Theory Comput.* **2019**, *15*, 6850−6858.
(74) Beckmann, R.; Brieuc, F.; Schran, C.; Marx, D. Infrared Spectra at Coupled Cluster Accuracy from Neural Network Representations. *J. Chem. Theory Comput.* **2022**, *18*, 5492−5501.
(75) Zhang, Y.; Ye, S.; Zhang, J.; Hu, C.; Jiang, J.; Jiang, B. Efficient and Accurate Simulations of Vibrational and Electronic Spectra with Symmetry-Preserving Neural Network Models for Tensorial Properties. *J. Phys. Chem. B* **2020**, *124*, 7284−7290.
(76) Thrift, W. J.; Ronaghi, S.; Samad, M.; Wei, H.; Nguyen, D. G.; Cabuslay, A. S.; Groome, C. E.; Santiago, P. J.; Baldi, P.; Hochbaum, A. I.; et al. Deep Learning Analysis of Vibrational Spectra of Bacterial Lysate for Rapid Antimicrobial Susceptibility Testing. *ACS Nano* **2020**, *14*, 15336−15348.
(77) Zhang, C.; Zhou, L.; Zhao, Y.; Zhu, S.; Liu, F.; He, Y. Noise reduction in the spectral domain of hyperspectral images using denoising autoencoder methods. *Chemom. Intell. Lab. Syst.* **2020**, *203*, 104063.
(78) Unke, O. T.; Chmiela, S.; Sauceda, H. E.; Gastegger, M.; Poltavsky, I.; Schütt, K. T.; Tkatchenko, A.; Müller, K.-R. Machine Learning Force Fields. *Chem. Rev.* **2021**, *121*, 10142−10186.
(79) Keith, J. A.; Vassilev-Galindo, V.; Cheng, B.; Chmiela, S.; Gastegger, M.; Müller, K.-R.; Tkatchenko, A. Combining Machine Learning and Computational Chemistry for Predictive Insights Into Chemical Systems. *Chem. Rev.* **2021**, *121*, 9816−9872.
(80) Morawietz, T.; Artrith, N. Machine learning-accelerated quantum mechanics-based atomistic simulations for industrial applications. *J. Comput. Aided Mol. Des.* **2021**, *35*, 557−586.
(81) Westermayr, J.; Marquetand, P. Machine Learning for Electronically Excited States of Molecules. *Chem. Rev.* **2021**, *121*, 9873−9926.
(82) Gastegger, M.; Schütt, K. T.; Müller, K.-R. Machine learning of solvent effects on molecular spectra and reactions. *Chem. Sci.* **2021**, *12*, 11473−11483.
(83) Gastegger, M.; Behler, J.; Marquetand, P. Machine learning molecular dynamics for the simulation of infrared spectra. *Chem. Sci.* **2017**, *8*, 6924−6935.
(84) Meuwly, M. Atomistic Simulations for Reactions and Vibrational Spectroscopy in the Era of Machine Learning-Quo Vadis? *J. Phys. Chem. B* **2022**, *126*, 2155−2167.
(85) Gandolfi, M.; Rognoni, A.; Aieta, C.; Conte, R.; Ceotto, M. Machine learning for vibrational spectroscopy via divide-and-conquer semiclassical initial value representation molecular dynamics with application to N-methylacetamide. *J. Chem. Phys.* **2020**, *153*, 204104.
(86) Wilson, E. B.; Decius, J. C.; Cross, P. C.*Molecular Vibrations. The Theory of Infrared and Raman Vibrational Spectra*; McGraw-Hill, New York, 1955.
(87) Woodward, L. A.*Introduction to the Theory of Molecular Vibrations and Vibrational Spectroscopy*; Oxford University Press, Oxford, 1972.
(88) Califano, S.*Vibrational States*; Wiley: London, 1976.
(89) Kraka, E.; Zou, W.; Tao, Y. Decoding Chemical Information from Vibrational Spectroscopy Data: Local Vibrational Mode Theory. *WIREs: Comput. Mol. Sci.* **2020**, *10*, 1480.
(90) Konkoli, Z.; Cremer, D. A New Way of Analyzing Vibrational Spectra. I. Derivation of Adiabatic Internal Modes. *Int. J. Quantum Chem.* **1998**, *67*, 1−9.
(91) Konkoli, Z.; Larsson, J. A.; Cremer, D. A New Way of Analyzing Vibrational Spectra. II. Comparison of Internal Mode Frequencies. *Int. J. Quantum Chem.* **1998**, *67*, 11−27.
(92) Konkoli, Z.; Cremer, D. A New Way of Analyzing Vibrational Spectra. III. Characterization of Normal Vibrational Modes in terms of Internal Vibrational Modes. *Int. J. Quantum Chem.* **1998**, *67*, 29−40.
(93) Konkoli, Z.; Larsson, J. A.; Cremer, D. A New Way of Analyzing Vibrational Spectra. IV. Application and Testing of Adiabatic Modes within the Concept of the Characterization of Normal Modes. *Int. J. Quantum Chem.* **1998**, *67*, 41−55.
(94) Cremer, D.; Larsson, J. A.; Kraka, E.New Developments in the Analysis of Vibrational Spectra on the Use of Adiabatic Internal Vibrational Modes. In *Theoretical and Computational Chemistry*; Parkanyi, C., Ed.; Elsevier: Amsterdam, 1998; pp 259−327.
(95) Zou, W.; Cremer, D. Properties of Local Vibrational Modes: The Infrared Intensity. *Theor. Chem. Acc.* **2014**, *133*, 1451−1466.
(96) Zou, W.; Izotov, D.; Cremer, D. New Way of Describing Static and Dynamic Deformations of the Jahn-Teller Type in Ring Molecules. *J. Phys. Chem. A* **2011**, *115*, 8731−8742.

(97) Zou, W.; Filatov, M.; Cremer, D. Bond Pseudorotation, Jahn-Teller, and Pseudo-Jahn-Teller Effects in the Cyclopentadienyl Cation and its Pentahalogeno Derivatives. *Int. J. Quantum Chem.* **2012**, *112*, 3277−3288.
(98) Zou, W.; Cremer, D. Description of Bond Pseudorotation, Bond Pseudolibration, and Ring Pseudoinversion Processes Caused by the Pseudo-Jahn-Teller Effect: Fluoro Derivatives of the Cyclopropane Radical Cation. *Aust. J. Chem.* **2014**, *67*, 435.
(99) Cremer, D.; Pople, J. A. General Definition of Ring Puckering Coordinates. *J. Am. Chem. Soc.* **1975**, *97*, 1354−1358.
(100) Fleming, G. D.; Martinez, U.; Mallea, M. A.; Guerra, J. Raman spectroscopy, DFT computations and SERS induced decomposition of (2-chloroethylphosphonic acid) ethephon. *J. Spectrosc. Dyn.* **2014**, *2014*, 16.
(101) Wilson, E. B. Some Mathematical Methods for the Study of Molecular Vibrations. *J. Chem. Phys.* **1941**, *9*, 76−84.
(102) Zou, W.; Kalescky, R.; Kraka, E.; Cremer, D. Relating Normal Vibrational Modes to Local Vibrational Modes with the Help of an Adiabatic Connection Scheme. *J. Chem. Phys.* **2012**, *137*, 084114.
(103) Zou, W.; Cremer, D. C_2 in a Box: Determining its Intrinsic Bond Strength for the $X^1\sum^+_g$ Ground State. *Chem. Eur. J.* **2016**, *22*, 4087−4097.
(104) Cremer, D.; Kraka, E. From Molecular Vibrations to Bonding, Chemical Reactions, and Reaction Mechanism. *Curr. Org. Chem.* **2010**, *14*, 1524−1560.
(105) Kraka, E.; Larsson, J. A.; Cremer, D.Generalization of the Badger Rule Based on the Use of Adiabatic Vibrational Modes. In *Computational Spectroscopy*; Grunenberg, J., Ed.; Wiley: New York, 2010; pp 105−149.
(106) Kalescky, R.; Kraka, E.; Cremer, D. Identification of the Strongest Bonds in Chemistry. *J. Phys. Chem. A* **2013**, *117*, 8981−8995.
(107) Mayer, I. Charge, bond order and valence in the AB initio SCF theory. *Chem. Phys. Lett.* **1983**, *97*, 270−274.
(108) Mayer, I. Bond orders and valences from ab initio wave functions. *Int. J. Quantum Chem.* **1986**, *29*, 477−483.
(109) Mayer, I. Bond order and valence indices: A personal account. *J. Comput. Chem.* **2007**, *28*, 204−221.
(110) Kalescky, R.; Zou, W.; Kraka, E.; Cremer, D. Local Vibrational Modes of the Water Dimer - Comparison of Theory and Experiment. *Chem. Phys. Lett.* **2012**, *554*, 243−247.
(111) Kalescky, R.; Kraka, E.; Cremer, D. Local Vibrational Modes of the Formic Acid Dimer - The Strength of the Double H-Bond. *Mol. Phys.* **2013**, *111*, 1497−1510.
(112) Larsson, J. A.; Cremer, D. Theoretical Verification and Extension of the Mckean Relationship between Bond Lengths and Stretching Frequencies. *J. Mol. Struct.* **1999**, *485*−*486*, 385−407.
(113) Johnson, R.NIST Standard Reference Database Number 101. *NIST Computational Chemistry Comparison and Benchmark Database*, 2019. http://cccbdb.nist.gov/.
(114) Bak, O.; Borowski, P.Scaling Procedures in Vibrational Spectroscopy. In *Molecular Spectroscopy—Experiment and Theory: From Molecules to Functional Materials*; Koleżyński, A., Król, M., Eds.; Springer: New York, NY, USA, 2019; pp 49−95.
(115) Kesharwani, M. K.; Brauer, B.; Martin, J. M. L. Frequency and Zero-Point Vibrational Energy Scale Factors for Double-Hybrid Density Functionals (and Other Selected Methods): Can Anharmonic Force Fields Be Avoided? *J. Chem. Phys.* **2015**, *119*, 1701−1714.
(116) Witek, H.; Morokuma, K. Systematic study of vibrational frequencies calculated with the self-consistent charge density functional tight-binding method. *Int. J. Quantum Chem.* **2004**, *25*, 1858−1864.
(117) Zou, W.; Tao, Y.; Freindorf, M.; Cremer, D.; Kraka, E. Local Vibrational Force Constants - from the Assessment of Empirical Force Constants to the Description of Bonding in Large Systems. *Chem. Phys. Lett.* **2020**, *748*, 137337.
(118) Slocum, J. D.; Webb, L. J. Measuring Electric Fields in Biological Matter Using the Vibrational Stark Effect of Nitrile Probes. *Annu. Rev. Phys. Chem.* **2018**, *69*, 253−271.
(119) Fried, S. D.; Boxer, S. G. Measuring Electric Fields and Noncovalent Interactions Using the Vibrational Stark Effect. *Acc. Chem. Res.* **2015**, *48*, 998−1006.
(120) Fried, S. D.; Boxer, S. G. Electric Fields and Enzyme Catalysis. *Annu. Rev. Biochem.* **2017**, *86*, 387−415.
(121) Verma, N.; Tao, Y.; Zou, W.; Chen, X.; Chen, X.; Freindorf, M.; Kraka, E. A Critical Evaluation of Vibrational Stark Effect (VSE) Probes with the Local Vibrational Mode Theory. *Sensors* **2020**, *20*, 2358.
(122) Chai, J.-D.; Head-Gordon, M. Long-range corrected hybrid density functionals with damped atom-atom dispersion corrections. *Phys. Chem. Chem. Phys.* **2008**, *10*, 6615−6620.
(123) Dunning, T. H. Gaussian basis sets for use in correlated molecular calculations. I. The atoms boron through neon and hydrogen. *J. Chem. Phys.* **1989**, *90*, 1007−1023.
(124) Kendall, R. A.; Dunning, T. H.; Harrison, R. J. Electron affinities of the first-row atoms revisited. Systematic basis sets and wave functions. *J. Chem. Phys.* **1992**, *96*, 6796−6806.
(125) Lemos, N. A.*Analytical Mechanics*; Cambridge University Press, 2018.
(126) Hanson, M. D.; Readnour, J. A.; Hassanali, A. A.; Corcelli, S. A. Coupled Local-Mode Approach for the Calculation of Vibrational Spectra: Application to Protonated Water Clusters. *J. Phys. Chem. Lett.* **2021**, *12*, 9226−9232.
(127) Sibert, E. L. Modeling vibrational anharmonicity in infrared spectra of high frequency vibrations of polyatomic molecules. *J. Chem. Phys.* **2019**, *150*, 090901.
(128) Beć, K. B.; Grabska, J.; Huck, C. W. In silico NIR spectroscopy − A review. Molecular fingerprint, interpretation of calibration models, understanding of matrix effects and instrumental difference. *Spectrochim. Acta A Mol. Biomol. Spectrosc.* **2022**, *279*, 121438.
(129) McKean, D. C. Individual CH bond strengths in simple organic compounds: effects of conformation and substitution. *Chem. Soc. Rev.* **1978**, *7*, 399.
(130) Brand, W. A.; Coplen, T. B.; Vogl, J.; Rosner, M.; Prohaska, T. Assessment of international reference materials for isotope-ratio analysis (IUPAC Technical Report). *Pure Appl. Chem.* **2014**, *86*, 425−467.
(131) Senga, R.; Lin, Y.-C.; Morishita, S.; Kato, R.; Yamada, T.; Hasegawa, M.; Suenaga, K. Imaging of isotope diffusion using atomic-scale vibrational spectroscopy. *Nature* **2022**, *603*, 68−72.
(132) Zou, W.; Tao, Y.; Freindorf, M.; Makoś, M. Z.; Verma, N.; Cremer, D.; Kraka, E.*Local Vibrational Mode Analysis (LModeA. Computational and Theoretical Chemistry Group (CATCO)*; Southern Methodist University: Dallas, TX, USA, 2022.
(133) Delgado, A. A. A.; Humason, A.; Kalescky, R.; Freindorf, M.; Kraka, E. Exceptionally Long Covalent CC Bonds - A Local Vibrational Mode Study. *Molecules* **2021**, *26*, 950.
(134) Yannacone, S.; Freindorf, M.; Tao, Y.; Zou, W.; Kraka, E. Local Vibrational Mode Analysis of π-Hole Interactions between Aryl Donors and Small Molecule Acceptors. *Crystals* **2020**, *10*, 556.
(135) Oliveira, V. P.; Marcial, B. L.; Machado, F. B.; Kraka, E. Relating Bond Strength and Nature to the Thermodynamic Stability of Hypervalent Togni-Type Iodine Compounds. *ChemPlusChem.* **2021**, *86*, 1199−1210.
(136) Delgado, A. A. A.; Sethio, D.; Munar, I.; Aviyente, V.; Kraka, E. Local Vibrational Mode Analysis of Ion−Solvent and Solvent−Solvent Interactions for Hydrated Ca^{2+} Clusters. *J. Chem. Phys.* **2020**, *153*, 224303.
(137) Freindorf, M.; Kraka, E. Critical Assessment of the FeC and CO Bond strength in Carboxymyoglobin - A QM/MM Local Vibrational Mode Study. *J. Mol. Model.* **2020**, *26*, 281.
(138) Kraka, E.; Freindorf, M.Characterizing the Metal Ligand Bond Strength via Vibrational Spectroscopy: The Metal Ligand Electronic Parameter (MLEP). In *Topics in Organometallic Chemistry—New Directions in the Modeling of Organometallic Reactions*; Lledós, A., Ujaque, G., Eds.; Springer: Berlin, Heidelberg, 2020; Vol. *67*; pp 1−43.
(139) McCutcheon, M.; Freindorf, M.; Kraka, E. Bonding in Nitrile Photo−dissociating Ruthenium Drug Candidates − A Local Vibrational Mode Study. *J. Chem. Phys.* **2022**, *157*, 014301.

https://doi.org/10.1021/acs.jpca.2c05962
J. Phys. Chem. A 2022, 126, 8781−8798

(140) Cremer, D.; Kraka, E. Generalization of the Tolman Electronic Parameter: The Metal-Ligand Electronic Parameter and the Intrinsic Strength of the Metal-Ligand Bond. *Dalton Trans* **2017**, *46*, 8323−8338.
(141) Setiawan, D.; Kraka, E.; Cremer, D. Quantitative Assessment of Aromaticity and Antiaromaticity Utilizing Vibrational Spectroscopy. *J. Org. Chem.* **2016**, *81*, 9669−9686.
(142) Li, Y.; Oliveira, V.; Tang, C.; Cremer, D.; Liu, C.; Ma, J. The Peculiar Role of the Au_3 Unit in Au_m Clusters: σ-Aromaticity of the Au_5Zn^+ Ion. *Inorg. Chem.* **2017**, *56*, 5793−5803.
(143) Kalescky, R.; Kraka, E.; Cremer, D. Description of Aromaticity with the Help of Vibrational Spectroscopy: Anthracene and Phenanthrene. *J. Phys. Chem. A* **2014**, *118*, 223−237.
(144) Tao, Y.; Zou, W.; Cremer, D.; Kraka, E. Characterizing Chemical Similarity with Vibrational Spectroscopy: New Insights into the Substituent Effects in Monosubstituted Benzenes. *J. Phys. Chem. A* **2017**, *121*, 8086−8096.
(145) Tao, Y.; Zou, W.; Cremer, D.; Kraka, E. Correlating the Vibrational Spectra of Structurally Related Molecules: A Spectroscopic Measure of Similarity. *J. Comput. Chem.* **2018**, *39*, 293−306.
(146) Verma, N.; Tao, Y.; Marcial, B. L.; Kraka, E. Correlation Between Molecular Acidity (pka) and Vibrational Spectroscopy. *J. Mol. Model.* **2019**, *25*, 48.
(147) Kraka, E.; Freindorf, M.; Cremer, D. Chiral Discrimination by Vibrational Spectroscopy Utilizing Local Modes. *Chirality* **2013**, *25*, 185−196.
(148) Lyu, S.; Beiranvand, N.; Freindorf, M.; Kraka, E. Interplay of Ring Puckering and Hydrogen Bonding in Deoxyribonucleosides. *J. Phys. Chem. A* **2019**, *123*, 7087−7103.
(149) Tao, Y.; Zou, W.; Sethio, D.; Verma, N.; Qiu, Y.; Tian, C.; Cremer, D.; Kraka, E. In Situ Measure of Intrinsic Bond Strength in Crystalline Structures: Local Vibrational Mode Theory for Periodic Systems. *J. Chem. Theory Comput.* **2019**, *15*, 1761−1776.
(150) Nanayakkara, S.; Tao, Y.; Kraka, E. Capturing Individual Hydrogen Bond Strengths in Ices via Periodic Local Vibrational Mode Theory: Beyond the Lattice Energy Picture. *J. Chem. Theory Comput.* **2022**, *18*, 562−579.
(151) Nie, J.; Tian, F.; Zheng, B.; Wang, Z.; Zheng, P. Exploration of Metal-Ligand Coordination Bonds in Proteins by Single-molecule Force Spectroscopy. *Chem. Lett.* **2021**, *50*, 1667−1675.
(152) Elkholi, I. E.; Elsherbiny, M. E.; Emara, M. Myoglobin: From physiological roles to potential implications in cancer. *Biochim. Biophys. Acta Rev. Cancer* **2022**, *1877*, 188706.
(153) Exertier, C.; Milazzo, L.; Freda, I.; Montemiglio, L. C.; Scaglione, A.; Cerutti, G.; Parisi, G.; Anselmi, M.; Smulevich, G.; Savino, C.; et al. Proximal and Distal Control for Ligand Binding in Neuroglobin: Role of the CD Loop and Evidence for His64 Gating. *Nature* **2019**, *9*, 5326.
(154) Luyckx, E.; Van Acker, Z. P.; Ponsaerts, P.; Dewilde, S. Neuroglobin Expression Models as a Tool to Study Its Function. *Oxid. Med. Cell. Longev.* **2019**, 5728129.
(155) Keppner, A.; Maric, D.; Correia, M.; Koay, T. W.; Orlando, I. M. C.; Vinogradov, S. N.; Hoogewijs, D. Lessons from the post-genomic era: Globin diversity beyond oxygen binding and transport. *Redox Bio* **2020**, *37*, 101687.
(156) Olson, J. S. Lessons Learned from 50 Years of Hemoglobin Research: Unstirred and Cell-Free Layers, Electrostatics, Baseball Gloves, and Molten Globules. *Antioxid. Redox Signal.* **2020**, *32*, 228−246.
(157) Sun, H.-J.; Lee, W.-T.; Leng, B.; Wu, Z.-Y.; Yang, Y.; Bian, J.-S. Nitroxyl as Potential Theranostic in the Cancer Arena. *Antioxid. Redox. Signal.* **2020**, *32*, 331−349.
(158) Rose, J. J.; et al. A neuroglobin-based high-affinity ligand trap reverses carbon monoxide-induced mitochondrial poisoning. *J. Biol. Chem.* **2020**, *295*, 6357−6371.
(159) Fukuto, J. M.; Vega, V. S.; Works, C.; Lin, J. The chemical biology of hydrogen sulfide and related hydropersulfides: interactions with biologically relevant metals and metalloproteins. *Curr. Opin. Chem. Biol.* **2020**, *55*, 52−58.
(160) Fiocchetti, M.; Fernandez, V. S.; Montalesi, E.; Marino, M. Neuroglobin: A Novel Player in the Oxidative Stress Response of Cancer Cells. *Oxid. Med. Cell. Longev.* **2019**, 6315034.
(161) Lorenz-Fonfria, V. A. Infrared Difference Spectroscopy of Proteins: From Bands to Bonds. *Chem. Rev.* **2020**, *120*, 3466−3576.
(162) Bakels, S.; Gaigeot, M.-P.; Rijs, A. M. Gas-Phase Infrared Spectroscopy of Neutral Peptides: Insights from the Far-IR and THz Domain. *Chem. Rev.* **2020**, *120*, 3233−3260.
(163) Ferrante, C.; Batignani, G.; Pontecorvo, E.; Montemiglio, L. C.; Vos, M. H.; Scopigno, T. Ultrafast Dynamics and Vibrational Relaxation in Six-Coordinate Heme Proteins Revealed by Femtosecond Stimulated Raman Spectroscopy. *J. Am. Chem. Soc.* **2020**, *142*, 2285−2292.
(164) Jones, E. M.; Monza, E.; Balakrishnan, G.; Blouin, G. C.; Mak, P. J.; Zhu, Q.; Kincaid, J. R.; Guallar, V.; Spiro, T. G. Differential control of heme reactivity in alpha and beta subunits of hemoglobin: A combined raman spectroscopic and computational study. *J. Am. Chem. Soc.* **2014**, *136*, 10325−10339.
(165) Spiro, T. G.; Soldatova, A. V.; Balakrishnan, G. CO, NO and O_2 as vibrational probes of heme protein interactions. *Coord. Chem. Rev.* **2013**, *257*, 511−527.
(166) Buhrke, D.; Hildebrandt, P. Probing Structure and Reaction Dynamics of Proteins Using Time−Resolved Resonance Raman Spectroscopy. *Chem. Rev.* **2020**, *120*, 3577−3630.
(167) Ardiccioni, C.; Arcovito, A.; Della Longa, S.; van der Linden, P.; Bourgeois, D.; Weik, M.; Montemiglio, L. C.; Savino, C.; Avella, G.; Exertier, C.; et al. Ligand Pathways in Neuroglobin Revealed by Low-temperature Photodissociation and Docking Experiments. *IUCrJ.* **2019**, *6*, 832−842.
(168) Chung, L. W.; Sameera, W. M. C.; Ramozzi, R.; Page, A. J.; Hatanaka, M.; Petrova, G. P.; Harris, T. V.; Li, X.; Ke, Z.; Liu, F.; et al. The ONIOM Method and Its Applications. *Chem. Rev.* **2015**, *115*, 5678−5796.
(169) Freindorf, M.; Delgado, A. A. A.; Kraka, E. CO Bonding in Hexa− and Pentacoordinate Carboxy−Neuroglobin − A QM/MM and Local Vibrational Mode Study. *J. Comput. Chem.* **2022**, *43*, 1725−1746.
(170) Fick, R. J.; Liu, A. Y.; Nussbaumer, F.; Kreutz, C.; Rangadurai, A.; Xu, Y.; Sommer, R. D.; Shi, H.; Scheiner, S.; Stelling, A. L. Probing the Hydrogen-Bonding Environment of Individual Bases in DNA Duplexes with Isotope-Edited Infrared Spectroscopy. *J. Phys. Chem. B* **2021**, *125*, 7613−7627.
(171) Jiang, Y.; Wang, L. Modeling the vibrational couplings of nucleobases. *J. Chem. Phys.* **2020**, *152*, 084114.
(172) Jiang, Y.; Wang, L. Development of Vibrational Frequency Maps for Nucleobases. *J. Phys. Chem. B* **2019**, *123*, 5791−5804.
(173) Hithell, G.; Donaldson, P. M.; Greetham, G. M.; Towrie, M.; Parker, A. W.; Burley, G. A.; Hunt, N. T. Effect of oligomer length on vibrational coupling and energy relaxation in double-stranded DNA. *Chem. Phys.* **2018**, *512*, 154−164.
(174) Hithell, G.; González-Jiménez, M.; Greetham, G. M.; Donaldson, P. M.; Towrie, M.; Parker, A. W.; Burley, G. A.; Wynne, K.; Hunt, N. T. Ultrafast 2D-IR and optical Kerr effect spectroscopy reveal the impact of duplex melting on the structural dynamics of DNA. *Phys. Chem. Chem. Phys.* **2017**, *19*, 10333−10342.
(175) Hithell, G.; Shaw, D. J.; Donaldson, P. M.; Greetham, G. M.; Towrie, M.; Burley, G. A.; Parker, A. W.; Hunt, N. T. Long-Range Vibrational Dynamics Are Directed by Watson−Crick Base Pairing in Duplex DNA. *J. Phys. Chem. B* **2016**, *120*, 4009−4018.
(176) Sanstead, P. J.; Stevenson, P.; Tokmakoff, A. Sequence-Dependent Mechanism of DNA Oligonucleotide Dehybridization Resolved through Infrared Spectroscopy. *J. Am. Chem. Soc.* **2016**, *138*, 11792−11801.
(177) Le Sueur, A. L.; Horness, R. E.; Thielges, M. C. Applications of two-dimensional infrared spectroscopy. *Analyst* **2015**, *140*, 4336−4349.
(178) Peng, C. S.; Jones, K. C.; Tokmakoff, A. Anharmonic Vibrational Modes of Nucleic Acid Bases Revealed by 2D IR Spectroscopy. *J. Am. Chem. Soc.* **2011**, *133*, 15650−15660.

https://doi.org/10.1021/acs.jpca.2c05962
J. Phys. Chem. A 2022, 126, 8781−8798

(179) Ji, P.; Feng, X.; Oliveres, P.; Li, Z.; Murakami, A.; Wang, C.; Lin, W. Strongly Lewis Acidic Meta-Organic Frameworks for Continuous Flow Catalysis. *J. Am. Chem. Soc.* **2019**, *141*, 14878−14888.
(180) Tomasi, J.; Mennucci, B.; Cammi, R. Quantum Mechanical Continuum Solvation Models. *Chem. Rev.* **2005**, *105*, 2999−3094.
(181) Perakis, F.; De Marco, L.; Shalit, A.; Tang, F.; Kann, Z.; Kühne, T.; Torre, R.; Bonn, M.; Nagata, Y. Vibrational Spectroscopy and Dynamics of Water. *Chem. Rev.* **2016**, *116*, 7590−7607.
(182) Brünig, F. N.; Geburtig, O.; Canal, A. v.; Kappler, J.; Netz, R. R. Time-Dependent Friction Effects on Vibrational Infrared Frequencies and Line Shapes of Liquid Water. *J. Phys. Chem. B* **2022**, *126*, 1579−1589.
(183) Rehl, B.; Ma, E.; Parshotam, S.; DeWalt-Kerian, E. L.; Liu, T.; Geiger, F. M.; Gibbs, J. M. Water Structure in the Electrical Double Layer and the Contributions to the Total Interfacial Potential at Different Surface Charge. *J. Am. Chem. Soc.* **2022**, *144*, 16338−16349.
(184) Geiger, F.; Hartland, G. Sixty Years of Surface-Specific Spectroscopy. *J. Phys. Chem. B* **2022**, *126*, 6367−6371.
(185) Ohno, P. E.; Wang, H.-f.; Geiger, F. M. Second-order spectral lineshapes from charged interfaces. *Nat. Commun.* **2017**, *8*, 1032.
(186) Ma, E.; Geiger, F. M. Divalent Ion Specific Outcomes on Stern Layer Structure and Total Surface Potential at the Silica:Water Interface. *J. Phys. Chem. A* **2021**, *125*, 10079−10088.
(187) Ma, E.; Ohno, P. E.; Kim, J.; Liu, Y.; Lozier, E. H.; Miller, T. F.; Wang, H.-F.; Geiger, F. M. A New Imaginary Term in the Second-Order Nonlinear Susceptibility from Charged Interfaces. *J. Phys. Chem. Lett.* **2021**, *12*, 5649−5659.
(188) Yang, N.; Khuu, T.; Mitra, S.; Duong, C. H.; Johnson, M. A.; DiRisio, R. J.; McCoy, A. B.; Miliordos, E.; Xantheas, S. S. Isolating the Contributions of Specific Network Sites to the Diffuse Vibrational Spectrum of Interfacial Water with Isotopomer-Selective Spectroscopy of Cold Clusters. *J. Phys. Chem. A* **2020**, *124*, 10393−10406.
(189) Miliordos, E.; Aprà, E.; Xantheas, S. S. Optimal geometries and harmonic vibrational frequencies of the global minima of water clusters $(H_2O)_n$, n = 2−6, and several hexamer local minima at the CCSD(T) level of theory. *J. Chem. Phys.* **2013**, *139*, 114302.
(190) Yang, N.; Duong, C. H.; Kelleher, P. J.; McCoy, A. B.; Johnson, M. A. Deconstructing water's diffuse OH stretching vibrational spectrum with cold clusters. *Science* **2019**, *364*, 275−278.
(191) Vogt, E.; Kjaergaard, H. G. Vibrational Spectroscopy of the Water Dimer at Jet-Cooled and Atmospheric Temperatures. *Annu. Rev. Phys. Chem.* **2022**, *73*, 209−231.
(192) Yu, Q.; Bowman, J. M. Classical, Thermostated Ring Polymer, and Quantum VSCF/VCI Calculations of IR Spectra of $H_7O_3^+$ and $H_9O_4^+$ (Eigen) and Comparison with Experiment. *J. Phys. Chem. A* **2019**, *123*, 1399−1409.
(193) Groß, A.; Sakong, S. Ab Initio Simulations of Water/Metal Interfaces. *Chem. Rev.* **2022**, *122*, 10746−10776.
(194) Tao, Y.; Zou, W.; Kraka, E. Strengthening of Hydrogen Bonding With the Push-Pull Effect. *Chem. Phys. Lett.* **2017**, *685*, 251−258.
(195) Hansen, T. C. The everlasting hunt for new ice phases. *Nat. Commun.* **2021**, *12*, 3161.
(196) Nada, H. Pathways for the formation of ice polymorphs from water predicted by a metadynamics method. *Sci. Rep.* **2020**, *10*, 4708.
(197) Santiago, P. H. d. O.; Duarte, E. d. A.; Nascimento, É. C. M.; Martins, J. B. L.; Castro, M. S.; Gatto, C. C. A binuclear copper(II) complex based on hydrazone ligand: Characterization, molecular docking, and theoretical and antimicrobial investigation. *Appl. Organomet. Chem.* **2022**, *36*, No. e6461.
(198) Hu, S.-X.; Zou, W. Stable copernicium hexafluoride (CnF_6) with an oxidation state of VI+. *Phys. Chem. Chem. Phys.* **2021**, *24*, 321−325.
(199) Christopher, I. L.; Michalchuk, A. A. L.; Pulham, C. R.; Morrison, C. A. Towards Computational Screening for New Energetic Molecules: Calculation of Heat of Formation and Determination of Bond Strengths by Local Mode Analysis. *Front. Chem.* **2021**, *9*, 2296−2646.
(200) Kabir, M. P.; Orozco-Gonzalez, Y.; Hastings, G.; Gozem, S. The effect of hydrogen-bonding on flavin's infrared absorption spectrum. *Spectrochim. Acta A Mol. Biomol. Spectrosc.* **2021**, *262*, 120110.
(201) Altun, Z.; Bleda, E. A.; Trindle, C. Focal Point Evaluation of Energies for Tautomers and Isomers for 3-hydroxy-2-butenamide: Evaluation of Competing Internal Hydrogen Bonds of Types -OH···O = , -OH···N, -NH···O = , and CH···X (X = O and N). *Molecules* **2021**, *26*, 2623.
(202) Ferreira de Menezes, R.; Machado de Macedo, L. G.; Lopes Martins, J. B.; Pirani, F.; Gargano, R. Investigation of strength and nature of the weak intermolecular bond in NH_2 radical-noble gas atom adducts and evaluation of their basic spectroscopic features. *Chem. Phys. Lett.* **2021**, *769*, 138386.
(203) Stephan, M.; Dammann, W.; Burger, P. Synthesis and Reactivity of Dinuclear Copper(I) Pyridine Diimine Complexes. *Dalton Trans* **2022**, *51*, 13396−13404.
(204) Wilcox, S.; Sethio, D.; Ward, J. S.; Frontera, A.; Lindh, R.; Rissanen, K.; Erdélyi, M. Do 2-coordinate iodine (I) and silver (I) complexes form nucleophilic iodonium interactions (NIIs) in solution? *Chem. Commun.* **2022**, *58*, 4977−4980.
(205) Hasil, A.; Beck, D.; Schröder, D.; Pillet, S.; Wenger, E.; Woike, T.; Klüfers, P.; Schaniel, D. Pas de Deux of an NO Couple: Synchronous Photoswitching from a Double-Linear to a Double-Bent $Ru(NO)_2$ Core under Nitrosyl Charge Conservation. *Angew. Chem., Int. Ed.* **2022**, *61*, No. e202210671.
(206) Kornienko, N.; Ly, K. H.; Robinson, W. E.; Heidary, N.; Zhang, J. Z.; Reisner, E. Advancing Techniques for Investigating the Enzyme−Electrode Interface. *Acc. Chem. Res.* **2019**, *52*, 1439−1448.
(207) Kraka, E.; Freindorf, M.Chemical Bonding in Homogenous Catalysis—Seen Through the Eyes of Vibrational Spectroscopy. *Reference Module in Chemistry, Molecular Sciences and Chemical Engineering—Comprehensive Computational Chemistry*; Elsevier, Heidelberg, 2022; pp 1−27.
(208) Bloomer, B. J.; Clark, D. S.; Hartwig, J. F. Progress, Challenges, and Opportunities with Artificial Metalloenzymes in Biosynthesis. *Biochemistry* **2022**, DOI: 10.1021/acs.biochem.1c00829.
(209) Ebensperger, P.; Jessen-Trefzer, C. Artificial metalloenzymes in a nutshell: the quartet for efficient catalysis. *Biol. Chem.* **2022**, *403*, 403−412.
(210) Boike, L.; Henning, N. J.; Nomura, D. K. Advances in covalent drug discovery. *Nature Rev. Drug Disc.* **2022**, DOI: 10.1038/s41573-022-00542-z.
(211) Kraka, E.; Zou, W.; Tao, Y.; Freindorf, M. Exploring the Mechanism of Catalysis with the Unified Reaction Valley Approach (URVA) - A Review. *Catalysts* **2020**, *10*, 691.